Catalytic Materials for Lithium-Sulfur Batteries: Mechanisms, Design Strategies and Future Perspective

Hao Chen^{1,2}, Zhenzhen Wu¹, Mengting Zheng¹, Tongchao Liu,³ Cheng Yan², Jun Lu^{3*}, Shanqing Zhang^{1*}

- 1. Centre for Clean Environment and Energy, School of Environment and Science, Gold Coast Campus, Griffith University, Gold Coast 4222, Australia
 - 2. School of Mechanical, Medical & Process Engineering, Queensland University of Technology (QUT), Brisbane, Queensland 4000, Australia
 - 3. Chemical Sciences and Engineering Division, Argonne National Laboratory, Lemont, IL 60439, United States

Correspondence should be addressed to J. Lu (junlu@anl.gov) or S. Zhang (s.zhang@griffith.edu.au)

Abstract

Lithium-sulfur batteries (LSBs) are attractive candidates for post-lithium-ion battery technologies because of their ultrahigh theoretical energy density and low cost of active cathode materials. However, the commercialization of LSBs remains extremely challenging primarily due to poor cycling performance and safety concerns, which are inherently caused by low conductivity of S₈ and Li₂S, severe polysulfide shuttling, and high polarization by solid Li₂S₂/Li₂S deposition. Catalytic materials could facilitate the large-scale practical application of LSBs by overcoming all these challenges. In this review, we investigate the sulfur species evolution in LSBs and explore the roles of catalytic materials in charge/discharge processes, highlighting the catalysis of solid S₈ to liquid polysulfides and solid Li₂S₂ to Li₂S. Furthermore, we offer systematic strategies from atomic to macro levels, including defect engineering, morphology engineering and catalyst compositing, to enhance catalysis efficiency in terms of sulfur supercooling, fast charge transfer, thiosulfate generation, disulfide bond cleavage, tuneable Li₂S growth and Li₂S decomposition enhancement. The design and availability of the proposed catalytic materials will further advance LSB technology from coin cells and pouch cells to the subsequent commercialization scale.

Table of contents

1.	Introduction	3
2.	Sulfur species evolution in LSBs	5
3.	Catalysis mechanisms in LSBs	7
	3.1 Catalysis in S ₈ -Li ₂ S ₈ solid-liquid transition	8
	3.2 Catalysis in LiPSs-LiPSs liquid-liquid transition	10
	3.2.1 Strong chemisorption of LiPS species for fast charge transfer	11
	3.2.2 Strong chemisorption of LiPS species for thiosulfate generation	15
	3.2.3 Tailoring LiPSs molecular structure via disulfide (-S-S-) bond cleavage	16
	3.3 Catalysis in LiPSs-Li ₂ S ₂ /Li ₂ S liquid-solid transition	17
	3.3.1 Spatial control of Li ₂ S	18
	3.3.2 Enhanced Li ₂ S decomposition	20
	3.4 Catalysis in Li ₂ S ₂ -Li ₂ S solid-solid transition	22
4.	Strategies for improved catalysis efficiency	23
	4.1 Defect engineering	24
	4.2 Morphology engineering.	26
	4.3 Catalyst compositing	28
5.	Conclusion and perspective	30
Dε	eclaration of Competing Interest	34
Αc	cknowledgements	34
Re	eferences	35

1. Introduction

As one of the most promising candidates for energy storage systems, lithium-sulfur (Li-S) batteries (LSBs) stand out due to their high theoretical energy density of 2600 Wh kg⁻¹ and 2800 Wh L⁻¹.

Moreover, sulfur is a naturally abundant, low-cost, and environmentally friendly by-product of the petroleum. However, several intrinsic challenges hinder the full utilization of LSBs, including 1) the insulating nature of sulfur (S₈) (conductivity of 5×10^{-30} S cm⁻¹ at 25 °C) and lithium sulfide (Li₂S) (conductivity $\approx 10^{-13}$ S cm⁻¹ at 25 °C), (2) shuttling effect caused by dissolution of lithium polysulfide (LiPS) intermediates; (3) large volume changes of sulfur cathode, and (4) lithium dendrite growth. Despite the fact that superior LSB performance has been achieved since 2009 when Nazar et al. reported an LSB with good rate properties and cycling efficiency, most reported studies were evaluated under laboratory settings such as low sulfur loading, excessive lithium anode, and flooded electrolytes. In other words, practical tests of pouch cells are still far from commercial application. In attempts to practically implement LSBs, several requirements have been proposed including high sulfur loading (≥ 70 wt%), high areal sulfur loading (≥ 5 mg cm⁻²), low ratio of electrolyte to sulfur (E/S ≤ 4 µl/mg), large electrode size (≥ 1 cm²/cell), and safety guarantees. Undeniably, the battery performance of LSBs will be further enhanced under these required conditions.

A standard Li-S battery consists of a sulfur cathode, a lithium anode, and organic lithium salt-based electrolyte. After discharging, the active material S₈ is reduced to fully discharged state Li₂S as shown in the overall cell reaction S₈+16Li ↔ 8Li₂S, delivering a specific capacity of 1675 mAh g⁻¹ based on S₈. Afterward, the Li₂S is oxidized back to S₈ upon charging. The underlying Li-S chemistry of these conversions is complex because each conversion is a multi-step reaction and various LiPSs (e.g., Li₂S₈, Li₂S₆, Li₂S₄, and Li₂S₂) are generated. The intrinsic properties of S₈, Li₂S, and LiPSs in LSBs cause many challenges in battery running, such as sluggish reaction kinetics, huge volume change, sulfur species dissolution, shuttling effect, lithium corrosion, and electrolyte depletion.⁸ To solve these issues in LSBs, various strategies have been attempted, such as using host materials,⁹ binders,¹⁰⁻¹² functional separators¹³, and novel electrolytes (e.g. new electrolyte solvents, additives, and lithium salts).¹⁴ However, most of these methods focused on suppressing the existing issues by confined

approaches, LiPS absorptivity, and lithium anode protection, rather than solving them, and do not solve the sluggish reaction kinetics in Li-S chemistry, especially the transformation of solid-phase S₈ and Li₂S₂/Li₂S. Despite some success with high sulfur loading and prolonged cycling in LSBs, the inevitable large internal resistance and loss of active materials make it difficult to realize superior battery performance at commercial levels.

Inspired by strategies to enhance the reaction kinetics of aqueous LiPSs, catalysis concepts were introduced to investigate the electrocatalytic effects in LSBs several years ago. ^{15,16} Following this, research on catalytic effects in LSBs demonstrated a dramatic increase in the number of publications per year (see Fig.1), resulting in various types of catalytic materials explored as listed in Table 1. Although it is widely recognized that catalytic materials could successfully boost LSB performance, the principle for catalytic material design is still undetermined because of the poor understanding of the catalytic mechanisms. Therefore, a critical review of catalytic effects in LSBs is imperative. Commonly, most review articles in LSB focused only on the LiPS-LiPS liquid-liquid conversion that brings the shuttle effect and the LiPS-Li₂S₂/Li₂S liquid-solid conversion that contributes the most to the capacity; 17-19 while the other two steps involved in LSBs, which are the S₈-LiPS solid-liquid transition and Li₂S₂-Li₂S solid-solid transition, have been often undervalued. Yet, the vital roles of these two steps in achieving high-rate capability should be fully realized, and related catalysts developed towards the boosted conversion of these sulfur species should be well summarized to advance our understanding of the overall 4 stages in LSBs. 20,21 Furthermore, recently reported materials and strategies (e.g. embedded polar materials and single-atom catalysts) were not covered in these pioneering reviews.

Herein, in this review, we aim to take all the phase transitions of sulfur species into account and present a profound overview of catalytic effects in each transition, including in S₈-LiPS solid-liquid transition, LiPS-Li₂S₂/Li₂S liquid-solid transition, and Li₂S₂-Li₂S solid-solid transition. Moreover, we review and discuss the state-of-the-art advances in catalytic material design. After all, future perspectives toward catalytic material design will be made regarding high-energy-density LSBs. Note that the catalysis concept in this review may be different from that in

conventional catalysis reactions which only alter the activation energy of the reaction without changing the states of catalysts after reaction. However, in LSBs, researchers focus more on the sulfur species transition rather than the states of catalytic materials although the catalytic materials are believed to form some activated states and then catalyse the reactions. In other words, the transition states and catalytic mechanisms of catalytic materials in the LSBs are poorly understood. For the sake of convenience, we adopt a broader catalysis concept referring to the materials that enhance the redox kinetics and improve the reaction efficiency of LSBs in this review.

2. Sulfur species evolution in LSBs

A typical LSB adopting sulfur as a starting material involves a continuous sulfur species transition between S₈ and Li₂S during a discharge process. The discharge profile shows that the LSB usually has two or three discharge stages (depending on the electrolyte systems and reaction temperature) as shown in **Fig. 2**, and undergoes a solid-liquid-solid transition as the reaction proceeds.^{8,22} For the sake of convenience, the discharge process can be divided into four steps based on the phase change of sulfur species:^{8,23}

Step 1: S₈-Li₂S₈ solid-liquid two phase transition

$$S_8 + 2Li \leftrightarrow Li_2S_8$$
 2.39 V vs. Li^0/Li^+ (1)

During this step, the solid S_8 will react to form Li_2S_8 which is dissolved into liquid electrolyte, resulting in numerous voids in the cathode. Though the insulating nature of bulk S_8 , the conversion from S_8 to Li_2S_8 is relatively easy owing to the low activation energy of this step.²⁴ However, the backward reaction from Li_2S_8 to bulk S_8 requires high activation voltages to drive the redox process. Therefore, the backward reaction of this step is one of the controlling steps for high-rate capability in LSB_8 .^{20,25}

Step 2: LiPSs-LiPSs liquid-liquid single phase transition (Li₂S₈-Li₂S₆-Li₂S₄)

$$3Li_2S_8 + 2Li \leftrightarrow 4Li_2S_6 \ 2.37 \ V \ vs. \ Li^0/Li^+ (2)$$

$$2Li_2S_6 + 2Li \leftrightarrow 3Li_2S_4 \ 2.24 \ V \ vs. \ Li^0/Li^+ \ (3)$$

This step is a liquid-liquid single-phase transition from Li₂S₈ to low-order LiPSs Li₂S_X ($2 < X \le 6$). In this step, the dissolved LiPSs intermediates would increase the electrolyte viscosity, diffuse to the Li anode side to be reduced and then shuttle back to the cathode, causing the so-called "shuttling effect". The "shuttling effect" is one of the causes of low Coulombic efficiency and rapid capacity fading. However, looking at the advantages of these intermediates, the dissolution of the LiPSs enables more solid sulfur to participate in the electrochemical reaction, thereby enhancing sulfur utilization. To suppress the shuttling effect, it is essential to further accelerate LiPSs-LiPSs liquid-liquid transition in spite of relatively fast conversion between liquid phases. Furthermore, considering the fluidity of dissolved LiPSs, strong adsorption ability is necessary to seize these LiPSs intermediates.

Step 3: LiPSs-Li₂S₂ liquid-solid two phase transition

$$Li_2S_4 + 2Li \leftrightarrow 2Li_2S_2 \sim 2.2 V vs. Li^0/Li^+$$
 (4)

In this step, the low-order LiPS Li₂S₄ is reduced into insoluble Li₂S₂, causing a clear voltage dip due to the initial nucleation barrier of the solid Li₂S₂. With a large deposition of insulating Li₂S₂ covering the conductive matrix, the intercepted conductive pathway for active intermediates results in a much higher energy barrier, which is responsible for capacity fading and insufficient sulfur utilization.

Step 4: Li₂S₂-Li₂S solid-solid single phase transition

$$Li_2S_2 + 2Li \leftrightarrow 2Li_2S$$
 2.15 V vs. Li^0/Li^+ (5)

This step contributes to a 50% theoretical capacity, equalling 836 mAh g⁻¹. However, this transition is not well described in the literature because the Li₂S₂ is not a stable phase and cannot be detected easily. In this step, the kinetically slow solid-phase conversion and insulating nature of Li₂S₂/Li₂S products lead to high polarization. In this regard, the facilitated nucleation/growth of Li₂S₂/Li₂S products and controlled spatial homogeneity of sulfur species are vital to speed up this solid-solid single phase transition.²⁷

Note that the exact and precise transfer mechanism of sulfur species is still debated, and the real reaction pathway in LSBs is much more complex. In this regard, some key issues should be pointed out: (1) The polysulfide species have more types than the aforementioned ones. For example, some

unusual LiPSs including Li₂S₇, Li₂S₅ and Li₂S₃ can be simultaneously observed because of their close Gibbs free-energies and the complicated disproportionation or comproportionation reactions between LiPSs. 14,23 (2) Despite the drawbacks of shuttling effects, the LiPSs dissolution can form intrinsic redox mediators to activate the solid sulfur and Li₂S, thereby increasing sulfur utilization. 20 To this end, the dissolved LiPSs play essential roles in boosting electrochemical performance of the LSBs. (3) Though the dominant solid-liquid-solid conversion mechanism in typical LSBs, the solid-solid multiphasic transitions still exist in some systems including the small sulfur molecules S_{2-4} , 28,29 organosulfides containing short sulfur chains, 30,31 solid-state electrolytes, 32 and conformal coating. 33,34 In these systems, the LiPSs do not occur or are sparingly dissolved or insoluble in the electrolytes, thereby greatly expanding the electrolyte options. $^{35-37}$ Nevertheless, the direct transition from S_8 into Li₂S₂/Li₂S via a solid-solid pathway requires extremely high activation energy because of the insulating nature of these solid materials and sluggish diffusion in solid phases.

Based on the above analyses, each transition step of the sulfur species is crucial in determining the electrochemical performance of the LSBs. Therefore, the catalytic effects in each step will significantly accelerate the whole transition process of sulfur species.

3. Catalysis mechanisms in LSBs

Catalysis is a process that increases the reaction rate without modifying the overall standard Gibbs energy change in the reaction.³⁸ In the LSBs, catalysis refers to a process that enhances the redox kinetics and improve the reaction efficiency of Li-S chemistry as defined above. Thus, the catalytic materials in the LSBs include materials that could significantly boost the electrochemical conversion process of sulfur species. Irrespective of the solid-liquid-solid reaction pathway or solid-solid reaction pathway, understanding and controlling catalysis processes during each conversion step plays a key role in improving electrochemical performance of LSBs. However, most previous reviews only highlighted the catalytic effects involving LiPSs and Li₂S₂/Li₂S conversion although the solid sulfur conversion is one of the controlling steps for high rate capability of the LSBs.^{20,39} Therefore, in order to cover diverse phase conversions and different catalysis mechanisms in each step, we will review

the catalytic mechanisms in the LSBs in four divided steps based on the phase change of sulfur species.

3.1 Catalysis in S₈-Li₂S₈ solid-liquid transition

Sulfur has a very rich chemistry, with around 30 allotropes amongst which the cyclic α -octasulfur (α -S₈) with an orthorhombic structure is the most stable form in nature. When the temperature increases, the α -S₈ transforms to other allotrope types as shown in **Fig.3a**. Among these sulfur allotropes, the short-chain sulfur shows admirable electrochemical properties in terms of specific capacity, cycling stability, and high rate capability in LSBs due to the alleviation of the dissolution and shuttling problems of polysulfides. An In this case, besides conventional dimethoxyethane (DME)/dioxolane (DOL) electrolyte, novel electrolytes including carbonate-based electrolytes are compatible with the LSBs. However, considering the insulating nature of bulk sulfur and the thermodynamically unstable or metastable properties of short-chain sulfur allotropes, a polymeric host with strong chemical bonds or a conductive microporous carbon matric is always required to confine these sulfur species (as shown in **Fig.3b**). Although not reported to date, it would be interesting if the short-chain sulfur molecules can be stabilized or the starting materials α -S₈ could be transferred to short-chain sulfur molecules by catalytic materials.

Another issue associated with sulfur chemistry is the physical state of the sulfur element, which entails the sluggish kinetics in solid-liquid or liquid-solid transition. Recently, Cui et al. reported liquid sulfur in a supercooled state achieved by a catalytic substrate at room temperature with enhanced mobility and transition kinetics.⁴⁴ This liquid-like behaviour of sulfur as a charging product in the LSBs relies on the substrate including nickel (Ni), palladium (Pd), platinum (Pt), indium tin oxide (ITO) and cobalt sulfide (CoS₂) (**Fig. 4a**).⁴⁴ The formation of supercooled sulfur can be attributed to two main factors: 1) compare with strong binding forces between solid metal-containing substrate and electrolyte solution, weak interactions form between liquid sulfur (nonpolar) and metal-containing solid surface (polar), and between liquid sulfur and electrolyte solution (polar); 2) the liquid electrolyte has relatively small surface energy with both metal-containing solid surface and sulfur, leading to a large contact angle. The combination of the weak interaction and large contact

angle helps isolate the liquid sulfur from the electrode surface, thus minimizing heterogeneous nucleation. Conversely, the strong interaction between sulfur and sp² carbon substrate leads to the good wetting ability of sulfur on carbon surface and easy solidification of sulfur. Cui et al. further systematically investigated the reaction mechanisms of liquid sulfur, realized precise control of sulfur shapes, and demonstrated the sulfur growth behaviour on various two-dimensional (2D) materials. 45,46 Finally, a light-weight, three-dimensional (3D) Ni-based current collector was designed to control the deposition and catalytic conversion of sulfur species, and achieved high LSB performance. 25 It was demonstrated that the liquid state of sulfur enabled high mobility and fast phase transition, thus accelerating the redox chemistry and improving kinetics during battery cycling. Moreover, the dead Li₂S could also be catalytically decomposed by the as-prepared Ni-based current collector (**Fig.4b**). In contrast, the accumulation of insulating Li₂S and disconnected solid sulfur on the carbon substrate would block charge transport and cause active material loss (Fig.4c). On the Al substrate, a thin and dense oxidation layer (Al₂O₃) on the surface could weaken the adsorption of sulfur species on the interface (Fig.4d). As a result, impressively improved cycle performance and rate capability of the Ni foam-based electrode were achieved due to the chemisorption of polysulfides by the Ni framework and the accelerated kinetics between liquid sulfur and liquid polysulfides on the surface of the Ni electrode.

To date, more catalytic substrates have been reported to catalytically stabilize the liquid sulfur at room temperature, such as gold (Au), molybdenum disulphide (MoS₂), tungsten disulphide (WS₂), molybdenum diselenide (MoSe₂), and graphite. The unexpected liquid behaviours of sulfur show great potential for achieving better reversible capacity, faster reaction kinetics, and longer cycling life compared to solid sulfur, and also provide a new route to design catalytic materials for high-energy and long-life LSBs. More importantly, the liquid sulfur could form on the catalytic materials toward the end of charging, and reversibly reduce into LiPSs upon charging, demonstrating the catalysis effect on both the conversion of S₈ to LiPSs and its backward reaction. Note that the direct application of liquid LiPSs as a flowable catholyte for electrochemical energy storage has been demonstrated to be feasible, and the sulfur utilization and rate performance of LSBs can be

improved.^{47,48} However, the use of liquid LiPSs instead of liquid sulfur as starting materials still sacrifices much specific capacity.

To date, the catalytic effects in S_8 -Li₂ S_8 solid-liquid transition have been severely underestimated, and less efforts have been devoted to boosting battery performance via exploring and developing novel catalytic materials for S_8 -Li₂ S_8 conversion. The related research is still at the early stage, and this area is worth more focused effort. For example, the electrochemical behaviours of amorphous sulfur remain verified. Therefore, the rich sulfur chemistry provides various pathways to design catalytic materials to boost the S_8 -Li₂ S_8 transition.

3.2 Catalysis in LiPSs-LiPSs liquid-liquid transition

The liquid-liquid phase transition (typical Li₂S₈–Li₂S₆–Li₂S₄) step which is the source of the shuttling effect has been theoretically considered a relatively fast conversion in LSBs.⁴⁹ However, in practical LSBs where the sulfur concentrations are much higher than in theoretical conditions, the transformation of LiPSs will be delayed, causing an accumulation in the electrolyte and severe shuttling effects. The accumulation of LiPSs will increase the viscosity of the electrolyte, and block the reaction highway, causing large internal resistance. ^{20,50} Accordingly, an adsorption-catalysis strategy was proposed in this step. Specifically, the strong adsorption ability which is normally provided by polar surface, can aggregate the dissolved LiPSs around the catalytic materials. Then, the catalytic materials enhance the liquid-liquid redox kinetics and accelerate the LiPSs interconversion. Therefore, the adsorption ability and catalysis work synergistically to alleviate hazardous pileup and improve the LSB performance. In this regard, an ideal catalyst in this step should meet the following requirements: 1) high conductivity to enable fast electron exchange, 2) high adsorption ability for LiPSs aggregation, and 3) high catalysis efficiency for LiPSs transformation. In this section, we will introduce different catalytic mechanisms for LiPSs-LiPSs liquid-liquid transition. It should be noted that the aforementioned issues of LiPSs-LiPSs transition exist in both reduction and oxidation of LiPSs, and the explored catalytic materials in this section are effective in boosting both reduction and oxidation processes.

3.2.1 Strong chemisorption of LiPS species for fast charge transfer

To address the shuttle effect, physical blocking was proposed to trap the long-chain LiPSs during charge-discharge processes, such as porous carbonaceous materials.⁵¹ However, physical encapsulation is not effective enough to suppress the shuttling,^{52,53} while chemical adsorption can provide continuous affinity to the dissolved LiPSs. The deep exploration of materials to restrict the sulfur species redistribution via chemical adsorption and physical barriers has occasionally involved electrocatalysis since sulfur confinement and catalysis normally coexist to improve the cyclability and rate capability of LSBs. Catalytic materials with strong chemisorption can provide the following advantages:⁵⁴ 1) Strong adsorption can enrich the LiPSs at the electrochemical interface to speed up the reaction and enhance the reaction kinetics; 2) Strong adsorption can ensure strong electrical contact, thereby enhance electron and ion exchange; 3) Strong interaction with LiPSs can spatially and kinetically regulate the growth and distribution of S and Li₂S.

The enhancement of LiPSs-LiPSs liquid-liquid transition significantly relies on fast charge transfer. Conductive materials with polar surfaces have high conductivity for electrons, and show strong promise as catalytic materials. Among conductive materials, carbon materials with heteroatom doping and structural engineering are very applicable. One specific example to highlight the necessity of heteroatom doping and structural design was produced by Du et al. who reported hierarchical nitrogen-doped carbon nanocages (hNCNC) to encapsulate sulfur and serve as an interlayer in LSBs as shown in Fig.5a.⁵⁵ The nitrogen-doped sp² carbon delivered highly efficient catalytic function to LiPSs conversion, and the hierarchical porous structure suppressed the polarization effect. Alternate analogs to graphite and graphene, the emerged 2D black phosphorus (BP) presented distinctive properties of tunable direct bandgap, ultrahigh charge mobility, large specific surface area, and anisotropic structure, which was also effective for immobiling LiPSs and catalyzing LiPSs conversion.⁵⁶ The monolayer form of BP, few-layer phosphorene nanosheets (FLP), could lower the polarization, accelerate the redox reaction, and improve sulfur utilization in the battery (as shown in Fig.5b) ⁵⁷.

To further improve the conductivity and polarity of conductive catalysts, a co-doping strategy can combine the speciality of different atoms, and provide stronger adsorption to LiPSs. As shown in Fig.5c, a hollow porous B.N-co-doped graphitic carbon-Co composite (h-Co-BN-GC) was employed as a dual electrocatalyst to promote the redox of LiPSs reaction kinetics. 58 The synergy between N and B could accelerate the electrochemical reactions of LiPSs and facilitate LiPSs conversion. More examples of enhanced catalysis efficiency by co-doping further confirm the significance of heteroatom atoms in carbon materials to increase the polarity of conductive carbon materials and ensure strong chemical adsorption of LiPSs, such as N, B co-doped curved graphene nanoribbons (NBCGN), ⁵⁹ B,O co-doped multiwalled carbon nanotubes (CNTs), ⁶⁰ N, P co-doped 3D carbon hybrid, 61 and N, P co-doped nanospheres. 62 Another type of conductive materials is metal oxides. For example, Magnéli phase Ti_4O_7 exhibits bulk metallic conductivity as high as 2×10^3 S cm⁻¹ at 298 K and also high affinity for LiPSs via polar O-Ti-O units. In the presence of Ti₄O₇, the fraction of LiPS intermediates is significantly decreased at all states of discharge (reaching a max of 40% for Ti₄O₇ versus 87% for carbon, respectively) compared with a hydrophobic carbon host (Fig.5d).⁶³ In this regard, a wide range of conductive materials have been used to catalyse LSBs, including conductive polymers, ⁶⁴⁻⁷⁰ MXene, ^{71,72} and carbon nitride (C₃N₄). ^{73,74}

The success of metal oxides in LSBs has resulted in significant research attraction for transition metal compounds and greatly enriched the metal-based catalytic materials, such as metal sulphides, metal nitrides, metal phosphides, and metal carbides. Metal sulphides have sulfiphilic sites to interact with LiPSs and also higher electrical conductivity than metal oxides because of their delocalized electronic structures. For example, cobalt sulphides were reported with high conductivities (CoS₂⁸⁰: 6.7 x10⁵ S m⁻¹; Co₃S₄⁸¹:3.3×10⁵ S m⁻¹; Co₉S₈⁸²:1.36 S m⁻¹) and excellent electrocatalytic capability to LiPSs. Considering the highest conductivity among cobalt sulphides, sulfiphilic cobalt disulfide (CoS₂) was investigated as an efficient additive to achieve high discharge capacity at high rates, improve energy efficiency, and enhance cycling stability. The strong interfacial interaction between CoS₂ and LiPSs could favour the charge transfer from conductive matrix to adsorbed LiPSs (**Fig.6a**).

An interesting fact lies in metal sulphides is that they have two main crystal structures: two-dimensional (2D)-layered metal sulphides and pyrite-type metal sulphides. The 2D-layered metal sulphides normally contain two configurations, i.e. basal plane and edge sites, which exhibit different catalysis efficiency. Taking 2D XS_2 (X = W, Mo) nanosheets as examples, the unsaturated S atoms over the edge sites carry electronegativity for effective adsorption of LiPSs, and the presence of catalytic edge sites enhances the charge-transfer kinetics (**Fig.6b**).⁸³ However, the structure type of sulphides does not determine the catalysis efficiency because both 2D-layered and pyrite-type metal sulphides effectively accelerate surface-mediated redox reactions and catalyse reduction /oxidation in LSBs as seen in a comparison of six different types of metal sulphides including VS_2 , CoS_2 , TiS_2 , FeS, SnS_2 , and Ni_2S_3 .³⁹

Metal phosphides, carbides and nitrides have superior properties including metallic conductivities, rapid surface reaction, and good catalytic properties. ^{84,85} Most recently, metal phosphides, carbides, nitrides, and borides have been widely investigated as emerging catalytic materials for LSBs, such as Ni₂P, ⁸⁶ Co₂P, ⁸⁶ Fe₂P⁸⁶, TiC, ^{84,87} W₂C, ⁸⁷ Mo₂C, ^{87,88} Fe₃C, ⁸⁹ TiN, ⁹⁰ VN, ^{91,92} Co₄N, ⁹³ titanium vanadium nitride (TVN), ⁹⁴ MgB₂, ⁹⁵ CoB, ⁹⁶ and Co₂B. ^{97,98} With respect to metal phosphides, the P atoms present strong electronegativity, enabling tuneable conductivity if adjusting the P/metal ratio. ⁸⁵ For instance, nickel (Ni)-rich phosphide (Ni₁₂P₅) shows a higher electron conductivity (500 S·m⁻¹) when compared with Ni-poor phosphide (Ni₂P). ⁹⁹ This tuneable strategy can be used to rationally design highly effective phosphide catalysts. In terms of the catalytic mechanisms, the band structure of the metal atoms in phosphides also plays a vital role in catalysing Li-S chemistry. The p band centre of P atom in CoP shows an upshift with respect to Fermi level, thus reducing energy gap between the cobalt 3d and P 2p band centres. This band shift facilitates the electron exchange to promote interfacial S₆²/S²-redox dynamics (**Fig.6c**). ¹⁰⁰

The aforementioned metal-based catalytic materials show their specific advantages. E.g., the metal phosphides, which can be synthesized by facile and gentle preparation procedures, show metallic characteristics and even superconductivity, ^{85,101} while the metal carbides and metal borides have relatively low molar weights, which is necessary to prepare lightweight catalysts. ¹⁰² As for metal

nitrides, they generally hold superior physicochemical stability over their oxide and sulfide counterparts.⁹⁴ Metal phosphides, borides, carbides, and nitrides, however, have low adsorption ability to LiPSs due to the low polarity of their anionic species compared with metal oxides and metal sulfides. Nanostructure design has been employed to maximize the binding sites and enhance the binding forces with LiPSs. For example, Zhong et al. designed a porous carbon fibres/vanadium nitride array (PCF/VN) composite scaffold for high-performance LSBs (as shown in **Fig.6d**).¹⁰³ The porous VN arrays exhibited good affinity and the strong chemical absorbing ability for LiPSs, provided fast electron transport pathways for active materials, and also prominently accelerated the electrochemical reaction kinetics.

Besides improving charge transfer via intrinsic conductive properties, the charge transfer can also be enhanced by fast surface diffusion. One specific example is transition metal compounds to catalyse the LSBs. Because of the poor conductivity of most metal oxides, there is no direct electron transfer between these metal oxides and LiPSs. Instead, the absorbed LiPSs are transferred to the conductive substrate and undergo the electrochemical reaction. Therefore, the competitive surface diffusion and adsorption of LiPSs determines the catalytic efficiency of metal oxides in LSBs. In particular, the weak capture capability to LiPSs would cause massive LiPSs dissolution and severe shuttling effect (Fig.7a), whereas excessively strong chemisorption would cause sluggish charge transfer and Li₂S growth (Fig.7c). Thus, balanced chemisorption and surface diffusion are necessary to achieve the optimized catalytic effects (Fig.7b).¹⁰⁴

In order to elucidate the effect of surface diffusion of metal oxides on catalytic effects, Tao et al. systematically investigated the catalytic mechanisms of various nonconductive metal oxides in LSBs and set up selection criteria for oxide catalytic materials. ¹⁰⁴ Firstly, the dominant monolayer chemisorption of oxides to LiPSs was confirmed. Secondly, these metal oxides functioned as transfer stations of LiPSs from poorly conductive oxide surfaces to a highly conductive carbon matrix. Thirdly, metal oxide could control Li₂S growth on the composite surface. Among selected nonconductive metal oxides (MgO, Al₂O₃, CeO₂, La₂O₃, and CaO), MgO, La₂O₃ and CeO₂ showed simultaneous strong binding and good surface diffusion, whereas Al₂O₃ exhibited the strongest

adsorption but slow diffusion. As a result, the composite cathode materials based on the MgO/C, La₂O₃/C and CeO₂/C nanoflakes showed higher capacity and better cycling performance (**Fig.7d**). These proposed selection criteria can also be generally employed for other materials such as metal sulfides, metal nitrides, and metal chlorides.

3.2.2 Strong chemisorption of LiPS species for thiosulfate groups and polythionates generation

Another well-acknowledged catalytic mechanism of LiPSs conversion relies on mediating polysulfide redox through insoluble thiosulfate species in a two-step process. First, the formed LiPSs are oxidized to insoluble thiosulfate groups on the surface by catalytic materials (Fig.8a). Then, the surface thiosulfate groups anchor the newly formed LiPSs by catenating them to form polythionates via "Wackenroder reaction" and converting them to solid Li₂S₂/Li₂S (Reaction 1 in Fig.8b). The polythionate complex could also be formed with only one -SO₃ group (Reaction 2 in Fig.8b). Therefore, the polythionate complex works as a transfer mediator to curtail LiPSs loss and supress the shuttling effect during cycles. ¹⁰⁵ This mechanism was first evidenced by MnO₂ (Fig.8a). ¹⁰⁵ After investigating a series of oxides, a "Goldilocks" principle was proposed to guide catalytic material selection and design by Liang et al. (Fig.8c). ¹⁰⁶ Specifically, metal oxides with a redox potential below approximately 1.5 V (such as Co₃O₄ or Ti₄O₇) show no redox reaction with LiPSs and mainly catalyse LiPSs conversion via strong chemisorption as mentioned above. Those with a redox potential in a target window (2.4 V < $E \le 3.05$ V) including VO₂, MnO₂, and CuO can oxidize LiPSs to form thiosulfate/polythionate groups as a reversible mediator. Catalytic materials with a high redox potential of above 3.05 V (such as V₂O₅ and NiOOH) oxidize LiPSs to form inactive sulfate groups which block the following redox reaction. However, the detrimental sulfate can be avoided by using a lower charge-off voltage. For example, the V₂O₅ can also be an effective catalytic material in a potential window range of 1.8-2.5 V. The "Goldilocks" principle paves a new way for better understanding catalytic mechanisms and exploring new catalytic materials.

The thiosulfate/polythionate mediator mechanism can be extended to more catalytic materials, including the hydroxyl (-OH) group terminated materials and metal sulfides. 83,105,107 For instance, the catalytic mechanism in OH terminated Mxene can be summarized as a dual-mode behaviour in which

the cleavage of OH groups was first achieved by the formation of the thiosulfate species, followed by a Lewis acid-base interaction between Ti atoms and polysulfides (Fig.8d).¹⁰⁷ This dual polysulfide adsorption mode could effectively suppress the LiPSs shuttle and regulate the uniform Li₂S deposition, leading to excellent electrochemical performance of Li-S batteries with high sulfur loading. Currently, the cleavage of the OH groups has been reported in -OH terminated MXene and -OH grafted graphene. ^{105,107} Whether it can be extended to other catalytic materials with -OH group still needs further systematic investigation. On the other hand, the polythionate complexes could also be detrimental if irreversible polythionate are formed in catalytic materials (such as conventional carbon-based electrodes). The formation of such irreversible reactions leads to a loss of active material, significantly affecting the cycle life of a battery. ⁸³ Therefore, it is vital to design catalytic materials with hydrophilic properties, which could create thiosulfate/polythionate groups when the hydroxyl groups are subject to the redox activity with LiPSs, thereby realizing reversible catalytic reactions and excellent long-term cycling performance of Li-S batteries with high sulfur loading.

3.2.3 Tailoring LiPSs molecular structure via disulfide (-S-S-) bond cleavage

In a typical LSBs system, the LiPSs follow a $S_8^{2-}S_6^{2-}S_4^{2-}S_2^{2-}$ conversion order during the discharge process. However, the LSBs may undergo a different conversion pathway in the presence of catalytic materials. For example, instead of transferring to S_4^{2-} , the S_6^{2-} can be split into two S_3^- radicals via disproportionation reaction, 108 which has a beneficial effect on increasing sulfur utilization. 109 The S_3^- radical can lower the large nucleation overpotential of solid Li_2S , driving further precipitation of Li_2S . 110 However, the S_3^- radical is usually induced and stabilized by highly solvating electrolytes rather than typical ether-based electrolytes. 110,111 Despite the essential roles of S_3^- radical in achieving high energy-density LSBs, the existing of S_3^- radicals induced by catalytic materials is rarely reported. An interesting study was conducted by Ding et al. who confirmed the presence of S_3^- radicals during catalysis using novel biomimetic molecule catalysts synthesized by grafting hemin molecules to three functionalized carbon nanotube systems (CNTs–COOH, CNTs–OH, and CNTs–NH₂). 112 As shown in **Fig.9a-c**, the catalytic material CNTs–COOH@hemin contained a lower concentration of S_8^{2-} and S_6^{2-} , but a relatively higher S_3^{--} radical concentration than other catalytic materials. The S_3^{--} radical was generated by S_6^{2-} or S_5^{2-} splits, and then underwent an electrochemical

reduction to form LiS₃ or Li₂S₃ (**Fig.9d**). This radical pathway for LSBs could greatly suppress the shuttling effect, leading to improved long-term cycling performance. The S₃⁻⁻ radical was also cross-validated by Na-S batteries when using the activated carbon cloth (ACC) as a catalytic substrate. This free-radical catalysis process mainly accelerates the redox conversion of intermediate polysulfide radical monoanions to lower-order polysulfides (S₃⁻⁻ \rightarrow S₂²⁻).

In addition to the S_3^- radical, the long-chain LiPSs can be sliced into other small LiPSs by "catalytic scissors". Inspired by biological catalysts used to rapidly slice disulphide (-S-S-) bonds, Yang et al. designed a porous carbon nanotube/S cathode (PCNTs-S) coupled to a lightweight graphene/dithiothreitol (Gra/DTT) interlayer, where the introduced DTT could rapidly eliminate the accumulation of LiPSs via the reaction to slice the -S-S- bonds. The DTT could slice a S_8^{2-} molecule to form $S_6^{2-}+S_2^{2-}$ or two S_4^{2-} species (**Fig.9e**), and then the S_4^{2-} species could form solid Li₂S or Li₂S₂ at room temperature. This -S-S- bond cleavage essentially circumvented the problem relating to the shuttle effect of soluble LiPSs, ensuring the long-term stable operation of Li-S batteries even at ultrahigh rates. This molecular scissor principle offers a promising avenue to speed up LiPSs conversion via transferring long-chain LiPSs to short chain LiPSs.

The rational control of LiPSs molecular structure via catalytic material can change the LiPSs conversion pathway. The most effective way for an ideal catalytic material is directly transforming one S_8^{2-} molecule into four S_2^{2-} molecules. Determining whether this powerful catalytic material will affect the reverse process from Li₂S to S_8 would be an interesting project.

3.3 Catalysis in LiPSs-Li₂S₂/Li₂S liquid-solid transition

The conversion from dissolved LiPSs to final product Li₂S contributes almost three-quarters (1254 mAh g⁻¹) of the theoretical capacity of the LSBs. ¹¹⁵ However, the sluggish deposition kinetics and uncontrolled growth of solid Li₂S is a critical obstacle to achieving complete sulfur utilization. In routine ether electrolytes, the film-like 2D growth of electronically and ionically insulating Li₂S causes electrode passivation and large polarization, leading to severe irreversible loss of active sulfur species and rapid capacity decay. In order to speed up redox kinetics involving Li₂S conversion, significant amounts of research have been devoted to electrolyte optimization. ^{110,116} However, the

extreme reactivity of aprotic electrolytes or additives with lithium metal and the exacerbated shuttling effect pose a serious challenge to stable cycling.¹¹⁶ To facilitate the deposition/dissolution of Li₂S, a range of chemisorption and/or catalysis strategies have been investigated with two main mechanisms proposed: spatially control the Li₂S growth and enhance Li₂S decomposition.

3.3.1 Spatial control of Li₂S

Three issues associated with the deposition of sulfur species should be considered ¹¹⁷: 1) The random deposition of S or Li₂S on the electrode surface results in large agglomerates of active materials that are electrochemically inert; 2) The slow redox kinetics of the LiPSs-Li₂S₂/Li₂S conversion bring in low sulfur utilization; 3) the solid S and Li₂S might bind weakly and detach away from the electrode surface and lose electrochemical activity. As a result, catalytic materials have been explored to strongly bond with sulfur species and control the deposition of the Li₂S.

The first method to regulate Li₂S deposition is bonding with polysulfides on the exposed sites and then inducing Li₂S deposition on the binding sites. For example, conductive tin-doped indium oxide coated carbon nanofibers (ITO-C) could provide many more deposition sites for LiPSs than pure C nanofibers alone, leading to much smaller Li₂S particles formed on the ITO-C surface (**Fig.10a-f**). The ITO nanoparticles work as anchors to locate the polysulfides on the surface, thereby promoting their redox kinetics and deposition efficiency.¹¹⁷ Additionally, the Li₂S deposition shows different chemical reactivity when exposed to the terrace and edge sites in 2D materials, so the study of the catalytic effects of different atomic sites on crystal surfaces is critical to understand the working mechanisms of 2D catalytic materials at atomic levels. Taking MoS₂ as an example, the MoS₂ edge sites have much higher electrochemical selectivity and activity than its terrace surface, leading to much more Li₂S deposited on the edge sites (**Fig.10g-h**). Therefore, the Li₂S nanoparticles can be induced to be randomly distributed on the whole surface area by designing horizontally grown MoS₂ sheets (**Fig.10i-j**).¹¹⁸ The demonstration of electrochemical selectivity of edge versus terrace sites provides clear guidance on material design for spatial control of Li₂S.

Instead of directly inducing Li₂S deposition, another way is to mediate the LiPSs rather than the Li₂S to control the Li₂S growth considering that the properties of the LiPSs greatly determine the

deposition rate and growth dimension of Li_2S on the conductive substrates. Therefore, catalytic materials which are chemically reactive to LiPSs have been explored to mediate the LiPSs and subsequently control the Li_2S growth. As a proof of concept, Zhao et al. introduced an organopolysulfide, di-t-butyl disulfide (DtbDS) as a redox comediator in LSBs. The DtbDS is chemically reactive and can react with LiPSs to form lithium t-butyl polysulfide (LitbPS) species. The generated LitbPSs further regulate the deposition of Li_2S from 2D to three-dimensional (3D) through a strengthened chemical decomposition/disproportionation pathway, leading to a 5-fold increase in the discharge capacity (**Fig.11a-b**). 120

Similar to thiosulfate groups catenating LiPSs to form polythionates via "Wackenroder reaction, 105" electrochemically active mediators which are inert to LiPSs in initial states but reactive to LiPSs after electrochemical activation have been investigated. Considering that two electrochemically distinct steps exist during discharge processes, in which the one at ~2.5 V is attributed to the interconversion of S₈ and Li₂S₄, and another one at ~2.1 V is attributed to the interconversion of Li₂S₄ and Li₂S, the key point to design the LiPS mediator is the careful matching of the mediator's electrochemical potential to either of these interconversion events. This design principle can be regarded as another "Goldilocks" principle. Benzo[ghi]peryleneimide (BPI) and polyimide-polyether (PIPE) are good examples to illustrate this principle. 121,122 BPI undergoes a single-electron reduction in a voltage range of 1.8-2.8 V, leading to an open-shell radical anion (BPI'). The diffusion and circulation of the generated BPI into the catholyte solution reduces the LiPSs to Li2S onto either Li2S or carbon surfaces, resulting in 3D morphologies (Fig.11c). 121 Similarly, two single-electron-transfer steps could be identified in a PIPE mediator, corresponding to the reduction reactions from neutral to mono-anion (r₁PIPE) at 2.46 and 2.33 V, and from r₁PIPE to dianion (r₂PIPE) at 2.01 and 1.9 V vs. Li/Li⁺, respectively. The redox potential ranges of PIPE are almost within the entire charge/discharge potential windows of sulfur in ether-based electrolytes, which are usually at 2.3-2.4 V (polysulfide/S₈) and 2.0-2.1 V (Li₂S/polysulfide) vs. Li/Li⁺, respectively. The presence of PIPE exhibited faster deposition rates and higher nucleation density of Li₂S, featuring the typical three-dimensional growth (Fig.11d). 122 More importantly, these catalytic materials normally are mobile in the electrolyte, which

can achieve ideal contact with immobile solid phases such as sulfur and Li₂S₂/Li₂S. This unique feature makes these mediators outstanding in facilitating solid-phase-involved redox reactions, such as the formation of Li₂S and its inverse oxidation. To design an ideal mediator for LSBs, some key requirements should be taken into consideration: 1) The extrinsic mediator should be redox-active in the operating window of the Li-S battery, ensuring that the mediator can reduce all sulfur species to Li₂S; 2) The extrinsic mediator should possess fast diffusion and conversion ability to promote the overall redox reactions; 3) The extrinsic mediators should achieve a full-range mediation of the whole multiphase Li-S reactions rather than only a specific electrochemical process; 4) The extrinsic mediator should be constrained from the lithium anode, avoiding its shuttling and lithium anode corrosion.

3.3.2 Enhanced Li₂S decomposition

The decomposition of Li₂S to Li₂Ss is a reverse conversion of Li₂Ss to Li₂S. Many catalytic materials which promote the reduction reaction of Li₂S to Li₂S can effectively catalyse the oxidation of Li₂S to LiPS₈, such as co-doped carbon, ¹²³ TiN, ¹²⁴ CoS₂, ²⁰ and TiS₂. ¹²⁵ It is reasonable to consider that if a catalytic material can accelerate the solid-liquid transformation by speeding up reactions of liquid LiPSs intermediates, the decreased LiPSs concentration favours the Li₂S oxidation reaction thermodynamically. In other words, the solid-liquid transformation from Li₂S to LiPSs can be indirectly accelerated by the catalytic materials. ²⁰ For example, considering the insulating and electrochemically inactive nature of Li₂S, conductive materials which have been proven to be effective to catalyse the conversion process from LiPSs to Li₂S should also be promising to enhance Li₂S oxidation. As a proof of concept, Zhang et al. investigated the nitrogen and phosphorus co-doped carbon (N, P-C) framework to enhance the redox kinetics of Li₂S cathodes. The porous 3D N, P-C framework could provide continuous electron pathways and hierarchically porous channels for Li ion transport. Meanwhile, P doping in the carbon framework plays an important role in improving the reaction kinetics, as it may help catalyse the redox reactions of sulfur species to reduce electrochemical polarization, and enhance the ionic conductivity of Li₂S. ¹²³ For better comparison of catalytic mechanisms involving Li₂S evolution, this section will mainly focus on the catalytic mechanisms based on Li₂S decomposition.

The catalytic mechanisms based on Li₂S decomposition have been primarily investigated in LSBs using Li₂S as the starting material. The large particle size of commercial Li₂S and the coarse Li₂S/carbon interface usually lead to a harsh activation process and lower sulfur utilization. ¹²⁶ In addition to conductivity enhancement, lowering the activation potential of Li₂S cathode can significantly improve its conversion efficiency. A broad spectrum of electrolyte additives have been trialled to activate Li₂S decomposition, such as phosphorus pentasulfide (P₂S₅), ¹²⁷ ammonium iodide (NH₄I), ¹²⁸ LiI, ¹²⁹ InI₃, ¹³⁰ In₂O₃, ¹³¹ and others ^{119,121}. The working mechanism of these additives is derived from strong interaction between the additives and Li₂S which results in reduced cell resistance and enhanced surface oxidation of Li₂S to LiPSs. ¹²⁷ Although these additives have high efficiency for lowering the charge over-potential, their mobile and corrosive redox mediators causes degradation of the Li anode. ¹³⁰

Recently, single atomic catalysts (SACs), an emerging catalytic material, have shown promising ability in LSBs and their working mechanism of SACs has been thoroughly investigated. As shown in Fig.12a, the SAC catalyst firstly coordinates with a Li₂S molecule, leading to a weakened Li-S bond. Then, one Li-S bond breaks and releases a Li ion. Meanwhile, the remaining SAC-[S-Li] species interacts with another Li₂S molecule, resulting in continuous release of Li ions and polysulfide chain growth. When the chain is long enough, the polysulfide chain will be released from the SAC surface. 132 Additionally, the lithium ion diffusion barrier on the carbon surface can also be decreased by the SACs. For example, Wang et al. embedded a single atomic Co (SACo) catalyst into Li₂S nanocomposite and reported that the energy of the delithiation of Li₂S was lowered in the presence of SACo (Fig.12b). 133 More importantly, the SACs could greatly improve the density of states (DOS) of the electrode at the Fermi level. The increased DOS means more electron occupation at the Fermi level, leading to higher electrical conductivity and promoted electrochemical reactions. 21 It should be noted that the SACs can also help chemically immobilize the soluble LiPSs and dynamically propel their fast conversion to insoluble end products (S or Li₂S).¹³⁴ According to the Lewis acid-base theory, the electron transfer from polysulfides anions to the metal-containing active center of the SACs could form strong meatal-S bonds, leading to a reduced energy barrier for the LiPSs conversion. 135 To date.

many types of SACs have been explored, such as manganese (Mn) single-atom, ¹³⁶ Zinc (Zn) single-atom. ¹³⁷ The biggest challenge in SACs catalysts is stabilizing their structure since the metal atoms in single-atom state tend to aggregate, which dramatically reduces their activity in electrochemical processes. ¹³⁸

3.4 Catalysis in Li₂S₂-Li₂S solid-solid transition

Although it is an important intermediate product, Li₂S₂ is yet to receive similar attention to other LiPSs because of its thermodynamical instability and spontaneous transformation to Li₂S plus S via disproportionation reaction in LSBs. 21,139,140 In most cases, Li₂S₂ is deemed as the final discharge product together with Li₂S. However, this solid-solid conversion of Li₂S₂/Li₂S holds the potential to deliver the last 50% theocratical capacity, equalling to a capacity of 836 mAh g⁻¹. ¹⁴¹ Unfortunately, as a semiconductor, Li_2S_2 is not capable of transporting free electrons, and the reduction reaction of Li₂S₂ to Li₂S is kinetically slow.^{21,139} The large positive Gibbs free energy for the formation of Li₂S from Li₂S₂ indicates that this conversion is the rate-limiting step in the whole discharge process.²¹ The sluggish conversion and insulating nature of Li₂S₂/Li₂S entail high overpotential and poor sulfur utilization, leading to a huge deviation between the practical capacity delivered and theoretical value. To this end, catalysts play a vital role in boosting the utilization of sulfur by providing active sites for deceasing the dissociation of Li₂S₂ and propelling the electrochemical reduction reaction. Also, the regulated nucleation/growth of Li₂S₂/Li₂S products and controlled spatial homogeneity of sulfur species can also contribute to speed up this solid-solid phase transition. Though few studies have examined this solid-solid transition, crucial achievements have been outlined and summarised in this section.

Many catalytic materials which effectively catalyse the dissolved LiPSs can also interact with solid Li_2S_2 intermediate, such as $\text{Co}_9S_8^{75,142}$ and single nickel (Ni) atoms on nitrogen-doped graphene (Ni@NG). As shown in **Fig.13a-b**, in the presence of Ni@NG catalytic material, the electron density of oxidized Ni sites ensures much charge transfer from the Li_2S_2 to the unfilled d orbital of single Ni atoms by chemical interaction, resulting in a decreased free energy of Li_2S_2 and enhanced kinetic conversion of the redox reaction. To investigate the catalytic effects on $\text{Li}_2S_2/\text{Li}_2S$

conversion, Yang et al. adopted a catalyst of amorphous cobalt sulfide (CoS₃) to decrease the dissociation energy of Li₂S₂ and propel the electrochemical transformation of Li₂S₂ to Li₂S. The adsorption energy (E_a) of Li₂S₂ on CoS₃ (-3.47 eV) was much stronger than the E_a of Li₂S₂ on the carbon nanotube (-2.39 eV), suggesting a strong interaction between polysulfides and CoS₃. Additionally, the lower dissociation energy (ΔE) of Li₂S₂ on CoS₃ and an increased distance of the S-S bond indicated the powerful effect of CoS₃ in catalysing the interconversion of Li₂S₂ to Li₂S. Thus, the LSBs exhibited high sulfur utilization, fast capacity output, and good cycling performance due to the lower dissociation energy of Li₂S₂ on the surface of CoS₃ and boosted conversion efficiency of Li₂S₂ to Li₂S (**Fig.13c**). ¹⁴³

Additionally, many pioneering works have demonstrated the feasibility of facilitating the conversion kinetics and sulfur utilization via controlled growth of these insulating sulfur species. ^{116,117}

Fundamentally, the morphologically engineered structure (normally 3D architecture) will facilitate fast charge transfer and prevent the growth of insulating lithium sulfide layer, therefore avoiding the passivation of sulfur cathodes. Though tremendous efforts are needed, adapting this strategy to design catalysts for solid-solid conversion of Li₂S₂/Li₂S will advance our knowledge and potentially boost the performance of LSBs in practical use.

Overall, the lack of Li₂S₂ research leads to an incomplete understanding of the roles of Li₂S₂ in LSBs, and the current research involving Li₂S₂-Li₂S conversion is mainly based on computational calculations. The weak signature of Li₂S₂ in experiments has posed great challenges for the verification of the catalytic mechanisms. Therefore, it is necessary to develop more powerful characterizations to unravel the roles of catalytic materials on the Li₂S₂/Li₂S solid-solid transition.

4. Strategies for improved catalysis efficiency

The redox reactions in LSBs are multi-step and multi-phase processes in which specific issues will be triggered, and each conversion step will significantly influence the following reactions. As high catalysis efficiency is vital in kinetically boosting the redox reactions and improving the electrochemical performance of the LSBs, in this section, the strategies for increasing catalysis efficiency will be introduced from the atomic level to the macro level.

4.1 Defect engineering

Defect engineering can effectively enhance ionic diffusion and electronic conductivity because the introduction of defects can narrow band gaps and provide additional energy levels.¹⁴⁴ Additionally, the defects in nonpolar materials can improve the surface polarization, leading to enhanced absorption ability to LiPSs in the LSBs. More importantly, the surface defects can facilitate the formation of free-radicals, which accelerates the conversion of LiPSs.⁵⁴ In LSBs, the catalytic materials mainly focus on three types of defects: oxygen defect, sulfur defect and nitrogen defect.

Oxygen defects are commonly reported in oxide catalysts, and can provide two advantages for these catalytic materials.⁵⁴ First, abundant oxygen defects act as the active centres participating in LiPSs adsorption. Second, oxygen defects can suppress the recombination of charge carriers due to the strong trapping ability for electron and hole, resulting in fast charge exchange. Taking perovskite-type La_{0.6}Sr_{0.4}CoO_{3-δ} (LSC) as an example, Sr doping can create abundant oxygen vacancies and valence variation of Co in the LSC, resulting in a largely improved conductivity of 52.63 S cm⁻¹ from 0.12 S cm⁻¹ in pristine LaCoO₃ (LCO). After Sr doping, the Co ions with mixed-valence show strong adsorption to the LiPSs (Li₂S₄ in **Fig.14a-b**). Specifically, the adsorption energies of Li₂S₄ are -2.59 eV on LSC (110) and -1.95 eV on LCO (110), which indicates that stronger interaction happens between Li₂S₄ and LSC (110) than between Li₂S₄ and LCO (110). The enhanced interaction strength between Li₂S₄ and LSC (110) was further evidenced by the peak shifts of XPS spectra (Fig.14c-d). 145 The advantages of oxygen defects have been demonstrated in other catalytic materials, such as TiO₂ nanosheets, ¹⁴⁶ La(OH)₃ nanorods, ¹⁴⁷ MnO₂ hollow nanospheres, ¹⁴⁸ Nb₂O_{5-x}, ¹⁴⁹ and Ti_nO_{2n-1} quantum dots. 150 However, in some cases, the existence of oxygen vacancies is detrimental to catalytic conversion. For example, the oxygen vacancies in layered niobic acid induced inferior performance of the LSBs due to the decreased electric conductivity and the weakened adsorption of LiPSs on the catalyst surface. In this case, oxygen vacancies are not universally effective in catalytic conversion. ¹⁵¹ Sulfur defects can create electron-rich surfaces for sulphides, facilitate the S radical formation, and improve catalytic efficiency through the following aspects 102: 1) Promoting the formation of sulfur anion radical (S_x') which can facilitate the reduction of sulfur to LiPSs;¹⁵² 2) Facilitating the

decomposition of long-chain LiPSs; 153 3) Accelerating the nucleation and deposition rate of Li₂S. 154 Herein, a sulfur-deficient Co₉S₈ catalytic material is presented as a proof of concept. As shown in **Fig.14e**, nanoparticles with a metallic Co₉S₈ core and a sulfur-deficient shell were decorated on the CNT surface. During the discharge-charge process, the polysulfide conversion could be catalysed by the sulfur-deficient shell which was supported by a robust crystalline Co₉S₈ core. Moreover, the intimate and electrically conducting interface between the Co₉S₈ core and CNT would facilitate charge separation and charge conduction from the reaction sites. 152 Interestingly, the catalytic mechanism of sulfur defects via metastable S_x species was proposed with the presence of MoS_{2-x}/rGO catalyst, 155 but this concept has not been verified with direct evidence. Therefore, the working mechanism of the sulfur defects in sulphides is still debated.

In addition to oxygen defect and sulfur defect, some novel defect types have recently been investigated, including nitrogen (N) defect, ^{156,157} and selenium (Se) defect. ¹⁵⁸ Besides these anion defects, some cation defects have been reported recently. The cation defects can not only improve electron and Li-ion conductivity of catalytic materials (e.g., titanium (Ti) defect), ¹⁵⁹ but also empower abundant adsorption sites to LiPSs and catalytic sites to accelerate the LiPSs conversion (e.g., Fe defect). ¹⁶⁰ Recently, a case study of cation defects was reported by Li et al. ¹⁶¹ In this study, a cation-vacancy-rich bimetallic oxide ZnCo₂O₄ was synthesized by partly replacing Co with Zn and *in-situ* etching of the Co₃O₄ model. The as-prepared ZnCo₂O₄ nanosheet exhibited a large amount of Zn vacancies that could effectively boost the anchoring and catalytic effects of the ZnCo₂O₄ nanosheet, thereby significantly suppressing the shuttle effect of Li-S batteries. As a result, the Li-S batteries with the Zn-vacancy-rich ZnCo₂O₄ nanosheet could achieve an ultrahigh loading of 21.06 mg cm⁻² with a high areal capacity of 13.95 mAh cm⁻². This study paves a new pathway to design vacancy-rich catalytic materials for high-performance Li-S batteries with high sulfur loading.

The introduction of vacancies can effectively enhance the adsorption ability to LiPSs and provide more active sites to boost LiPSs conversion. However, some concerns should be taken into consideration in terms of the application of defect engineering¹⁰²: 1) The vacancy sites and vacancy concentration should be optimized through rational design to yield maximum catalysis efficiency; 2)

The working mechanisms of vacancies need more exploration via more advanced characterizations.

There are some strategies reported previously to rationally design the defects of catalytic materials, such as down-sizing of catalytic materials, chemical reduction and etching, physical exfoliation and etching, and element doping. ¹⁶² Each method has its specific application area. For example, the down-sizing of catalytic materials is effective in creating intrinsic defects, while heteroatom doping can induce different types of defects. As for physical exfoliation, it is widely used to control the defects in 2D materials. ¹⁶³ In terms of defect characterizations, many advanced technologies have been explored, including aberration-corrected high-resolution TEM (HRTEM), high-angle annular dark-field imaging (HAADF), extended X-ray absorption fine structure (EXAFS), positron annihilation spectroscopy (PAS), and X-ray absorption fine structure (XAFS) spectroscopy. ¹⁶³ These advanced characterizations can help researchers obtain in-depth information about defects even at the atomic level and explain the positive effect of defects on catalysis processes.

4.2 Morphology engineering

As discussed above, the catalytic efficiency of catalysts is highly determined by the active sites and mass/charge exchange rate. The rational control of catalyst morphology is considered an effective strategy to realize selectivity of the exposed active sites and high exchange rate of mass/charge. In this regard, the optimization of the existing catalytic materials via morphology engineering is vital to maximizing catalysis efficiency. The morphology engineering of catalysts can be generally divided into a crystalline structure, nano-structure and micro-structure from different dimensions. In this section, we introduce morphology engineering of catalytic materials in LSBs at different levels.

The rational design of crystal structure mainly involves the selectivity of the exposed facets in the catalytic materials considering that the different exposed planes have unique chemical and electronic structures.⁸³ The search for effective exposed active sites primarily focuses on noble metals and 2D transition metal dichalcogenides^{25,83} with other materials systems (e.g., oxides, SACs) rarely reported. Thus, investigation of the effects of the crystal structures of these materials on the catalytic efficiency of LSBs would be an interesting avenue for research.

Nano-structure design can realize maximum utilization of catalytic materials by fully exposing the active catalytic sites. Following this strategy, the mass proportion of catalytic materials is normally reduced to nano-levels, such as CoP nanoflakes, 164 VN nanobelts, 103 VN nanoribbon, 91 TiC nanosheelts, ¹⁶⁵ Co₃S₄ nanotues, ⁷⁸ and CoSe nanopolyhedrons. ¹⁶⁶ These nanostructures aim to adsorb and catalyse the sulfur species through the relatively large surface area. For example, the nanotube morphology of Co₃S₄ helps to host sulfur species and enhance catalytic kinetics due to its high surface area (Fig.15a). Additionally, the Co₃S₄ nanotubes have a relatively lower percolation threshold than Co₃S₄ nanoparticles because of the large aspect ratio of nanotubes readily forming a conducting network. 78 Along this line, the extreme of reducing particle size is to reach the single-atom level, namely SACs. Theoretically, SACs possess the highest active site utilization and should be the ideal choice considering the utilization rate of catalytic sites. 167 However, a suitable substrate or host is normally necessary to hold SACs since a single atom is chemically unstable. 138 The nano-structure design has also been applied to conductive carbon hosts to improve electrical conductivity, such as Ndoped porous carbon cages, 168 vertically erected graphene nanoflake, 164 and N-doped carbon nanotubes. 169 The well-controlled carbon material provides a large mesoporous structure to achieve high sulfur content and the rampant electron transport pathways to obtain good electrical conductivity. Additionally, the physical encapsulation and good catalytic activity led to suppressed shuttling effect and boosted LiPSs conversion (Fig.15b). 168

Considering that sulfur species conversion involves electron and ion transfer, constructing robust 3D conductive pathways is also crucial to boosting the catalysis efficiency in LSBs. Generally, 3D carbon nanomaterials with a highly dense pore distribution and large specific surface area have been designed to provide high conductivity and sufficient space to host the sulfur and LiPSs and evenly disperse catalytic materials. For instance, He et al. designed a freestanding 3D graphene/1T MoS₂ (3DG/TM) heterostructure with highly efficient electrocatalysis properties for the LiPSs. The 3DG/TM composed of graphene/1T MoS₂ nanosheets was cross-linked to form a 3D interconnected network with rich pores (**Fig.16a**), which were beneficial for electrolyte penetration and Li-ion and electron transfer. Therefore, high electrocatalytic efficiency for LiPSs conversion was achieved due to the excellent

ion/electron transfer and the presence of sufficient electrocatalytic active sites. ¹⁷⁰ The 3D framework has also been designed to enlarge the contact area between catalytic materials and carbon matrix, providing fast transformation paths for electrons. As a proof of concept, Zhang et al. implanted ultrafine Ta₂O_{5-x} nanoclusters into the micropores of carbon nanospheres (a-Ta₂O_{5-x}/MCN) as an electrocatalyst in LSBs (**Fig.16b**). The elaborate design could bring in several advantages: 1) A "ship in a bottle" structure to guarantee a high surface-to-volume ratio to offer abundant polysulfide-retaining and catalytically active sites but also prevent the agglomeration of nanoclusters, thereby addressing the nanocatalyst stability issues; 2) The increased penetration of electrolytes and charge transfer due to the porous conductive network; 3) The porous structure of carbon nanospheres could improve sulfur homogenization and buffer sulfur volume expansion during cycling. ¹⁷¹ In summary, the 3D framework design could boost the catalysis process by speeding up charge transfer and dispersing the catalytic materials.

The well-designed frameworks would effectively confine the sulfur species and further enhance the capture capability for LiPSs. For example, layered double hydroxides (LDHs) composed of positively charged metal hydroxide layers and charge-balancing anions in the interlayer regions were decorated on reduced graphene oxide (rGO) nanosheet to construct a crepe cake framework. As shown in **Fig.16c**, sulfur nanoparticles were well-encapsulated between between LDH and rGO. This structure brought in several functions: 1) The sulfur species were effectively confined in the catalytic material via electrostatic force, polar interaction, Lewis acid—base bonding and hydrogen bonding; 2) The rGO layer provided fast electron transfer and buffered the volume expansion of sulfur during cycles; 3) LDH could significantly accelerate the conversion of LiPS and reduce the positive electrode polarization in the sulfur redox process.¹⁷²

4.3 Catalyst compositing

Different types of catalytic materials have different functionalities and advantages, and single-type catalysts always realize a single side of functionality, such as fast charge transfer by conductive catalytic materials and strong absorption ability by polar catalytic materials. In other words, most catalytic materials are not compatible with catalysing all conversion steps and have limitations. For

example, typical metal oxides demonstrate insufficient electrical conductivity while metal nitrides present relatively poor adsorption capacity to the LiPSs.⁵⁴ In response, combining two or more catalytic materials to integrate multiple functionalities could effectively improve the overall performance of catalytic materials.

To date, tremendous efforts have been devoted to designing heterostructure materials to achieve synergic effects of the catalytic materials. For example, MoS₂, a representative catalyst in LSBs, shows a low intrinsic electron conductivity, which will dramatically restrict the redox kinetics of S₈ ↔ Li₂S. To remedy this weakness of MoS₂, MoN-MoS₂ heterostructure was designed by Wang et al. 173 MoN was selected because it exhibits high intrinsic electron conductivity (4.55 × 10⁶ S m⁻¹). The working mechanism of MoS₂-MoN could be ascribed to "1+1>2" synergistic catalytic conversion mechanism (Fig.17a-b). In particular, the MoN with intrinsic high electron conductivity could provide the coupled electron to speed up the conversion from liquid LiPSs to solid Li₂S through the oxidation reaction with LiPSs. Meanwhile. MoS₂ with moderate absorption capability could regulate LiPSs around the cathode and provide fast Li⁺ diffusion paths with low diffusion energy barriers. Along this direction, many heterogeneous structures have been explored, such as TiO₂-TiN, ¹⁷⁴ TiN-Ti₄O₇, ¹⁷⁵ VO₂-VN₂, ¹⁷⁶ V₂O₃-V₈C₇, ¹⁷⁷ MoN-VN, ¹⁷⁸ WS₂-WO₃, ¹⁷⁹ VTe₂-MgO, ¹⁸⁰ NiO-NiCo₂O₄, ¹⁸¹ SnS₂-SnO₂, ¹⁸² ZnS-FeS, ¹⁸³ ZnS-SnS, ¹⁸⁴ and MoC-MoO_x. ¹⁸⁵ The heterostructure can also be between metal compounds and metal-free materials, e.g., TiC-graphene heterostructure, 165,186 ultrathin TiO_{2-x} nanosheets and carbon nanotubes (CNTs) heterojunction electrocatalysts.¹⁸⁷ In summary, constructing heterostructures for catalytic materials demonstrates some unique superiority including advanced interface formation and multicomponent functional collaboration. 102

The biggest challenge in constructing heterostructures is the compatibility of each part, which means the heterostructure is not universal for all these catalytic materials. For example, the SACs normally need a carbonaceous substrate to avoid their aggregation so that it is quite difficult to realize heterostructure on SACs. In this case, implanting these catalytic materials into a suitable host is a facile but effective strategy to realize the synergic effects of different catalytic materials. ⁸⁸ For instance, Zhao et al. proposed a cathode structure composed of uniformly embedded ZnS

nanoparticles and Co-N-C single-atom catalyst to form double-end binding sites inside a highly oriented macroporous host to realize good Li-S pouch cell performance. As shown in Fig.17c, the macroporous pores facilitated ionic transport to boost the sulfur utilization and the redox reaction kinetics under high sulfur loading and lean electrolyte operation. Additionally, the polar ZnS nanoparticles and Co-N-C SAC double-end binding (DEB) sites effectively immobilized and catalysed the LiPSs conversion and further avoided lithium anode corrosion. The synergistic functions of different parts could realize fast redox reaction kinetics and almost no shuttle effect in the LSBs. Accordingly, an A-h-level pouch cell was assembled to validate the advantages of the catalytic materials in high sulfur loading (~6 mg/cm²), thin Li anode (negative/positive capacity ratio of ~2.6), and lean electrolyte (4µl/mg) operation. As a result, the as-assembled cell delivered >1,200 mAh g⁻¹ at 41.67 mA g⁻¹ and achieved practical specific energy of 317 Wh kg⁻¹. More surprisingly, the A-h-level Li-S pouch cell still delivered high Coulombic efficiency (>95%) and stable cycling performance for 80 cycles (~74% capacity retention). The obtained high practical specific energy of over 300 W h kg⁻¹ and stable cycle life in pouch cells lessens the gap between the high theoretical specific energy of LSBs and their realization in practical systems.

Various catalytic materials take care of different aspects of high-performance LSBs. Conductive catalytic materials mainly contribute to fast charge transfer, and polar catalytic materials are mainly in charge of shuttle inhibition, while the dissoluble mediators in liquid electrolytes help spatial distribution control of soluble LiPSs and reactivation of dead active materials. Considering the complexity of sulfur species conversion in LSBs involving multiple-phase and multiple-step reactions, integration of multiple catalytic materials shows great promise to achieve smooth conversion for the entire landscape.

5. Conclusion and perspective

LSBs show great potential for next-generation energy-storage systems because of their high-energy density and the natural abundance of sulfur. Although laboratory tests of LSBs have achieved great progress in terms of cycle life and rate capability, the performance of pouch cells remains below the great expectations of the market. Several challenges, such as sluggish reaction kinetics, severe

shuttling effect, low sulfur loading, and flooded electrolytes need to be solved before Li-S could be the next commercial success after Li-ion batteries. The concept of catalysis effect has been proposed to solve these issues and construction of high-energy-density LSBs, and various catalytic materials have been explored. In this review, we have reported the catalysis mechanisms in each conversion step of Li-S chemistry and the latest development of catalytic materials in LSBs. The strategies of improving catalysis efficiency were also summarized.

The typical conversion pathway of sulfur species in LSBs can be divided into four main steps during discharging: solid S₈→liquid Li₂S₈, liquid Li₂S₈→liquid short-chain LiPSs, liquid short-chain LiPSs→ solid Li₂S₂, and solid Li₂S₂→solid Li₂S. Each step has its unique features which bring in specific issues. The conversion of solid S₈ to liquid Li₂S₈ requires high activation voltages due to the insulating nature of bulk sulfur and relatively sluggish solid-liquid phase transition. The process of liquid Li₂S₈ to liquid short-chain LiPSs leads to a severe shuttling effect, which is one of the reasons for low Coulombic efficiency and rapid capacity fading. The conversion of liquid short-chain LiPSs to solid Li₂S₂ requires large overpotential because of the initial nucleation barrier of the solid Li₂S₂ and the insulating Li₂S₂ covering the conductive matrix. The final step of Li₂S₂/Li₂S conversion leads to high polarization because of the kinetically slow solid-phase transformation and insulating nature of Li₂S₂/Li₂S products. With respect to these features and issues in each step, different catalytic materials have been designed, and corresponding working mechanisms have been investigated. Although there is significant difficulty in transferring solid S₈ into small molecular sulfur through catalysis, the discovery of supercooled sulfur makes the catalysis of solid S₈ to Li₂S₈ feasible for high-performance LSBs. The conversion processes between the liquid LiPSs have received increasing attention, and various catalytic materials have been designed, including metal-free catalysts, metal oxides, metal sulfides, metal nitrides, metal phosphides, metal carbides and SACs.

Considering the dissolution of LiPSs, the "adsorption-catalysis" principle has been proposed. In terms of catalysis mechanisms, three main strategies have been proposed: 1) Strong chemisorption of LiPS species for fast charge transfer; 2) Strong chemisorption of LiPS species for thiosulfate generation; 3) Tailoring LiPSs molecular structure via disulfide (-S-S-) bond cleavage. In the conversion process of

LiPSs to Li₂S₂/Li₂S and its reverse reaction, the spatial control of Li₂S and the enhancement of Li₂S decomposition are the main working mechanisms to catalyse this process. The final step of Li₂S₂ to Li₂S, which has been always overlooked, is one of the controlling steps for high rate capability in the LSBs. In this respect, it is necessary to explore more catalytic materials for Li₂S₂/Li₂S solid-solid transition.

Many strategies have been put forward to boost the catalysis efficiency. From the atomic level to the macro level, the catalysis efficiency can be boosted by defect engineering, morphology engineering, and catalyst compositing. The defect engineering is effective in enhancing ionic diffusion and electronic conductivity, and improving the surface polarization as well as creating more free radicals, which accelerate the LiPSs conversion. The rational morphology design of catalytic materials including crystal structure, nano-structure and macro-structure can selectively develop highly effective exposed active sites, maximize the catalytic active sites, and construct highly conductive pathways. Considering the limitations of single catalytic materials, composite catalytic materials could realize the synergistic effects of different catalytic materials, which could effectively improve the overall performance of catalytic materials in the LSBs. In summary, the catalysis effect could significantly accelerate the reaction kinetics and boost the electrochemical performance of LSBs.

Despite the considerable progress that has been made over the past few decades, there are still several challenges related to catalytic materials which have not yet been solved as well as more opportunities for discovering new catalytic materials for LSBs. Important issues that need further work include but are not limited to:

- (1) Although many catalysis mechanisms have been proposed, the in-depth understanding and validation of these mechanisms still require appropriate characterization techniques, especially *in-situ* characterizations, to observe the instantaneous change of sulfur species and catalytic materials. The full track of reaction processes is important to establish the fundamental theory to guide the exploration and design of catalytic materials.
- (2) The current research focuses more on the liquid-liquid and liquid-solid conversion processes in LSBs, while the conversion processes of solid S₈ to liquid LiPSs and solid Li₂S₂ to solid

- Li_2S have yet to receive much attention. The processes involving solid S_8 , Li_2S_2 and Li_2S conversion have been identified as the controlling steps for high rate capability in LSBs. Therefore, more catalytic materials and mechanistic understanding related to conversion processes of solid S_8 to liquid LiPSs and solid Li_2S_2 to solid Li_2S should be explored.
- (3) Cross-disciplinary research would provide creative methods to design highly effective catalytic materials. For example, biocatalysts inspired the development of chemical scission of S-S bonds which could rationally tailor the sulfur chains. Catalysis in other areas, including fuel cell and metal-air batteries, could provide inspiration to design catalytic materials for LSBs. Conversely, the research on catalytic materials for LSBs can also provide substantial guidance for some emerging energy storage systems, including Na-S batteries, Li-Se batteries, and Si-S batteries. Taking Na-S batteries as examples, the low operating temperatures, including the intermediate temperature (120-300 °C) and room temperature of Na-S batteries, are attractive future research directions considering the safety risks, high maintenance costs, and limited energy density of commercial high-temperature (300-350 °C) Na-S batteries. However, the sluggish reaction kinetics and shuttling behaviours of dissolved sodium polysulfides in low-temperature Na-S batteries are extremely unsatisfactory to achieve the full utilization of the active material sulfur and long-term cycling stability. In this regard, the exploration of catalytic materials for low-temperature Na-S batteries is necessary to accelerate the conversion of sodium polysulfides and guide the Na₂S deposition.
- (4) Solid-state LSBs have attracted increasing attention due to their promising theoretical energy density and high safety. When applying solid-state electrolytes, the slow reaction kinetics would get worse without LiPS as redox mediators for electrochemical oxidation and chemical dissolution of Li₂S. In this case, the catalytic materials would play a more important role in achieving high-performance solid-state LSBs. For instance, the functional materials (e.g., TiO₂, Al₂O₃, ceramic electrolytes) in solid-state electrolytes may not only improve the electrochemical performance of the solid-state electrolytes but also catalyse the sulfur species conversion. More importantly, the catalytic materials in solid-state batteries may boost the

properties of the lithium anode and mitigate the Li dendrite growth by suppressing polysulfide shuttle and improving the ionic conductivity of solid electrolytes. ¹⁹² Therefore, the catalytic materials are expected to achieve multiple functions for both solid-state electrolytes and sulfur cathodes. However, the research on catalytic materials for solid-state LSBs is still at an early stage, and more efforts should be made to understand their working mechanisms.

(5) The commercialization process of Li-S batteries has been hampered by harsh practical operation conditions under which the cycling stability and rate capability are still far from satisfactory. Catalytic materials exhibit great promise in solving the critical issues in Li-S chemistry, and the combination of different catalytic materials could greatly improve the overall performance of LSBs. Currently, the catalytic materials empower the Li-S pouch cells with ampere-hour-scale capacity, specific energy of up to 350 W h kg⁻¹, high coulombic efficiency (>95%), and stable cycling performance (74% capacity retention). 188 Once the fundamental requirements (e.g., high specific capacity, rate capability, and superior cycling stability) have been fulfilled by the catalytic materials under practical test conditions (e.g., lean electrolyte condition and high loading of sulfur), more efforts could be devoted to optimizing the cell configuration for further increasing the specific energy of LSBs. In addition, light-weight and compact voluminous high-energy configurations are required in the practical pouch cells. Therefore, catalytic materials with high efficiency, lightweight, low cost, and controllable structure are highly recommended. In this regard, the configuration of conductive carbon substrates and metal compounds (nitrides, metal oxides, and sulfides) is highly preferable.

Declaration of Competing Interest

The authors declare that they have no known competing financial interests or personal relationships that could have appeared to influence the work reported in this paper.

Acknowledgements

The work at Argonne National Laboratory was supported from the U. S. Department of Energy (DOE), Office of Energy Efficiency and Renewable Energy, Vehicle Technologies Office. Argonne

National Laboratory is operated for DOE Office of Science by UChicago Argonne, LLC, under contract number DE-AC02-06CH11357. This work was financially supported by the Australian Research Council (ARC) Discovery Projects (DP210103266 and DP1701048343), the Griffith University Publication Assistance Scholarship, and the Queensland University of Technology (QUT) Early Career Researchers (ECR) Seed Grant (323100-0518/07).

References

- 1. Chung, W. J., et al., Nat. Chem. (2013) 5 (6), 518
- 2. Bruce, P. G., et al., Nat. Mater. (2012) 11 (1), 19
- 3. Hong, X., et al., Adv. Mater. (2019) **31** (5), 1802822
- 4. Ji, X., et al., Nat. Mater. (2009) 8 (6), 500
- 5. Ye, Y., et al., Adv. Mater. (2017) 29 (48), 1700598
- 6. Park, J., et al., Nano Today (2018) 18, 35
- 7. Bhargav, A., et al., Joule (2020) 4 (2), 285
- 8. Xu, R., et al., Adv. Energy Mater. (2015) 5 (16), 1500408
- 9. Seh, Z. W., et al., Chem. Soc. Rev. (2016) 45 (20), 5605
- 10. Chen, H., et al., Chem. Rev. (2018) 118 (18), 8936
- 11. Hencz, L., et al., Nano-Micro Lett. (2019) 11 (1), 17
- 12. Chen, H., et al., J. Energy Chem. (2021) 62, 127
- 13. Jeong, Y. C., et al., Adv. Funct. Mater. (2018) 28 (38), 1707411
- 14. Zhang, S. S., J. Power Sources (2013) 231, 153
- 15. Babu, G., et al., Sci. Rep. (2015) 5 (1), 8763
- 16. Sun, F., et al., J. Mater. Chem. A (2013) 1 (42), 13283
- 17. Lim, W.-G., et al., Angew. Chem. Int. Ed. (2019) 58 (52), 18746
- 18. Liu, D., et al., Adv. Sci. (2018) 5 (1), 1700270
- 19. Zhang, Z.-W., et al., Adv. Funct. Mater. (2018) 28 (38), 1707536
- 20. Yuan, Z., et al., Nano Lett. (2016) 16 (1), 519
- 21. Du, Z., et al., J. Am. Chem. Soc. (2019) 141 (9), 3977
- 22. Su, Y.-S., et al., Nat. Commun. (2013) 4 (1), 2985
- 23. Yin, Y.-X., et al., Angew. Chem. Int. Ed. (2013) **52** (50), 13186
- 24. Peng, L., et al., Nat. Catal. (2020) 3 (9), 762
- 25. Zhou, G., et al., Sci. Adv. (2020) 6 (21), eaay5098
- 26. Li, J., et al., J. Energy Chem. (2021) 54, 434
- 27. Peng, H.-J., et al., J. Am. Chem. Soc. (2017) 139 (25), 8458
- 28. Xin, S., et al., J. Am. Chem. Soc. (2012) **134** (45), 18510
- 29. Li, Z., et al., Adv. Energy Mater. (2014) **4** (7), 1301473
- 30. Wei, S., et al., J. Am. Chem. Soc. (2015) 137 (37), 12143
- 31. Zhou, J., et al., Adv. Mater. (2017) 29 (33), 1701294
- 32. Yang, X., et al., Chem. Soc. Rev. (2020) 49 (7), 2140
- 33. Li, X., et al., Nano Lett. (2016) 16 (6), 3545
- 34. Li, X., et al., Nat. Commun. (2018) 9 (1), 4509
- 35. Warneke, S., et al., J. Electrochem. Soc. (2018) **165** (10), A2093
- 36. Yang, H., et al., Angew. Chem., Int. Ed. (2019) 58 (3), 791
- 37. Li, Q., et al., Energy Storage Mater. (2018) 14, 75
- 38. Laidler, K. J., Pure Appl. Chem. (1996) **68** (1), 149
- 39. Zhou, G., et al., Proc. Natl. Acad. Sci. (2017) 114 (5), 840
- 40. Meyer, B., Chem. Rev. (1976) **76** (3), 367

- 41. Peramunage, D., and Licht, S., Science (1993) **261** (5124), 1029
- 42. Wang, D.-W., et al., J. Mater. Chem. A (2013) 1 (33), 9382
- 43. Zhang, B., et al., Energy Environ. Sci. (2010) 3 (10), 1531
- 44. Liu, N., et al., Proc. Natl. Acad. Sci. (2019) 116 (3), 765
- 45. Zhou, G., et al., Nat. Commun. (2020) 11 (1), 606
- 46. Yang, A., et al., Nat. Nanotechnol. (2020) 15 (3), 231
- 47. Frischmann, P. D., et al., Chem. Mater. (2015) 27 (19), 6765
- 48. Pan, H., et al., Adv. Energy Mater. (2015) 5 (16), 1500113
- 49. Lu, Y.-C., et al., J. Phys. Chem. C (2014) 118 (11), 5733
- 50. Cañas, N. A., et al., Electrochim. Acta (2013) 97, 42
- 51. Wang, T., et al., Small Methods (2017) 1 (8), 1700089
- 52. Manthiram, A., et al., Nat. Rev. Mater (2017) 2 (4), 16103
- 53. Song, J., et al., Adv. Funct. Mater. (2014) **24** (9), 1243
- 54. Zhang, M., et al., Adv. Energy Mater. (2020) 10 (2), 1903008
- 55. Du, L., et al., Nano Energy (2019) 57, 34
- 56. Xu, Z.-L., et al., Nat. Commun. (2018) 9 (1), 4164
- 57. Li, L., et al., Adv. Mater. (2017) **29** (2), 1602734
- 58. Li, N., et al., Carbon (2019) **149**, 564
- 59. Chen, L., et al., J. Mater. Chem. A (2017) 5 (16), 7403
- 60. Jin, C., et al., J. Mater. Chem. A (2017) 5 (2), 632
- 61. Wu, H., et al., J. Mater. Chem. A (2017) 5 (38), 20458
- 62. Wang, J., et al., Adv. Sci. (2018) 5 (11), 1800621
- 63. Pang, Q., et al., Nat. Commun. (2014) 5 (1), 4759
- 64. Xiao, L., et al., Adv. Mater. (2012) 24 (9), 1176
- 65. Zhou, W., et al., J. Am. Chem. Soc. (2013) 135 (44), 16736
- 66. Yin, F., et al., Solid State Sci. (2017) 66, 44
- 67. Liang, X., et al., J. Power Sources (2011) **196** (16), 6951
- 68. Fu, Y., and Manthiram, A., J. Phys. Chem. C (2012) **116** (16), 8910
- 69. Yang, Y., et al., ACS Nano (2011) 5 (11), 9187
- 70. Li, W., et al., Nano Lett. (2013) **13** (11), 5534
- 71. Wang, X., et al., Angew. Chem. Int. Ed. Engl. (2021) 60 (5), 2371
- 72. Li, P., et al., Adv. Mater. (2021) **33** (17), 2007803
- 73. Wang, M., et al., Nano Research (2018) 11 (6), 3480
- 74. Liang, J., et al., ACS Appl. Mater. Interfaces (2016) 8 (38), 25193
- 75. Pang, Q., et al., Mater. Horiz. (2016) 3 (2), 130
- 76. Zhang, S. S., and Tran, D. T., J. Mater. Chem. A (2016) 4 (12), 4371
- 77. Sun, K., et al., J. Electrochem. Soc. (2015) 162 (14), A2834
- 78. Pu, J., et al., Nano Energy (2017) **37**, 7
- 79. Xu, J., et al., Adv. Sci. (2021) 8 (16), 2101019
- 80. Yomo, S., J. Magn. Magn. Mater. (1983) **31-34** (PART 1), 331
- 81. Bouchard, R. J., et al., Inorg. Chem. (1965) 4 (5), 685
- 82. Jana, M., et al., Nanotechnology (2015) 26 (7)
- 83. Babu, G., et al., J. Am. Chem. Soc. (2017) 139 (1), 171
- 84. Peng, H.-J., et al., Angew. Chem. Int. Ed. (2016) **55** (42), 12990
- 85. Yu, S., et al., J. Energy Chem. (2021) **55**, 533
- 86. Yuan, H., et al., ACS Energy Lett. (2017) 2 (7), 1711
- 87. Zhou, F., et al., Nano Lett. (2018) **18** (2), 1035
- 88. Niu, S., et al., Energy Storage Mater. (2020) **33**, 73
- 89. Pan, H., et al., J. Energy Chem. (2019) **39**, 101
- 90. Lim, W.-G., et al., Adv. Mater. (2019) **31** (3), 1806547
- 91. Sun, Z., et al., Nat. Commun. (2017) 8 (1), 14627

- 92. Song, Y., et al., ACS Appl. Mater. Interfaces (2019) **11** (6), 5687
- 93. Deng, D.-R., et al., ACS Nano (2017) **11** (6), 6031
- 94. Shang, C., et al., Adv. Energy Mater. (2021) 11 (3), 2003020
- 95. Pang, Q., et al., Joule (2019) 3 (1), 136
- 96. Li, Z., et al., Adv. Mater. (2021) n/a (n/a), 2102338

https://doi.org/10.1002/adma.202102338

- 97. Guan, B., et al., J. Mater. Chem. A (2018) 6 (47), 24045
- 98. Guan, B., et al., ACS Nano (2019) **13** (6), 6742
- 99. Yu, X.-F., et al., Nano Research (2019) **12** (5), 1193
- 100. Zhou, J., et al., Joule (2018) 2 (12), 2681
- 101. Zhang, W., et al., Nano Energy (2021) 90, 106475
- 102. Wang, P., et al., Adv. Energy Mater. (2021) **11** (7), 2002893
- 103. Zhong, Y., et al., Adv. Funct. Mater. (2018) 28 (38), 1706391
- 104. Tao, X., et al., Nat. Commun. (2016) 7 (1), 11203
- 105. Liang, X., et al., Nat. Commun. (2015) 6 (1), 5682
- 106. Liang, X., et al., Adv. Energy Mater. (2016) 6 (6), 1501636
- 107. Liang, X., et al., Adv. Mater. (2017) 29 (3), 1603040
- 108. Vijayakumar, M., et al., Phys. Chem. Chem. Phys. (2014) 16 (22), 10923
- 109. Zhang, G., et al., Angew. Chem. Int. Ed. (2018) 57 (51), 16732
- 110. Gupta, A., et al., Adv. Energy Mater. (2019) 9 (6), 1803096
- 111. Shyamsunder, A., et al., Angew. Chem. Int. Ed. (2017) 56 (22), 6192
- 112. Ding, X., et al., Adv. Funct. Mater. (2020) **30** (38), 2003354
- 113. Kumar, A., et al., ACS Energy Lett. (2020) 5 (6), 2112
- 114. Hua, W., et al., ACS Nano (2017) 11 (2), 2209
- 115. Pan, H., et al., Nat. Energy (2017) 2 (10), 813
- 116. Chu, H., et al., Nat. Commun. (2019) 10 (1), 188
- 117. Yao, H., et al., Nat. Commun. (2014) 5 (1), 3943
- 118. Wang, H., et al., Nano Lett. (2014) 14 (12), 7138
- 119. Meini, S., et al., J. Phys. Chem. Lett. (2014) 5 (5), 915
- 120. Zhao, M., et al., Chem (2020) 6 (12), 3297
- 121. Gerber, L. C. H., et al., Nano Lett. (2016) 16 (1), 549
- 122. Xie, J., et al., Angew. Chem. Int. Ed. (2020) **59** (40), 17670
- 123. Zhang, J., et al., Adv. Energy Mater. (2017) 7 (14), 1602876
- 124. Wang, Y., et al., Energy Storage Mater. (2019) 16, 228
- 125. Seh, Z. W., et al., Nat. Commun. (2014) 5 (1), 5017
- 126. Seh, Z. W., et al., Chem. Sci. (2013) 4 (9), 3673
- 127. Zu, C., et al., J. Phys. Chem. Lett. (2014) 5 (22), 3986
- 128. Pan, H., et al., ACS Appl. Mater. Interfaces (2017) 9 (5), 4290
- 129. Wu, F., et al., Adv. Mater. (2015) 27 (1), 101
- 130. Liu, M., et al., Nano Energy (2017) 40, 240
- 131. Hua, W., et al., Adv. Mater. (2021) 33 (38), 2101006
- 132. Wang, J., et al., Energy Storage Mater. (2019) 18, 246
- 133. Wang, J., et al., Energy Storage Mater. (2020) 28, 375
- 134. Li, Y., et al., Energy Storage Mater. (2020) **30**, 250
- 135. Zhang, L., et al., Adv. Mater. (2019) **31** (40), 1903955
- 136. Liu, Y., et al., Energy Storage Mater. (2021) **35**, 12
- 137. Xu, K., et al., Energy Storage Mater. (2019) **23**, 587
- 138. Wang, J., et al., ChemSusChem (2020) 13 (13), 3404
- 139. Liu, Z., et al., J. Phys. Chem. Lett. (2017) 8 (7), 1324
- 140. Park, H., et al., J. Phys. Chem. C (2015) 119 (9), 4675
- 141. Ji, X., and Nazar, L. F., J. Mater. Chem. (2010) 20 (44), 9821

- 142. Liu, Y., et al., Adv. Funct. Mater. (2020) **30** (32), 2002462
- 143. Yang, X., et al., Adv. Mater. (2019) 31 (25), 1901220
- 144. Su, Z., et al., Electrochemical Energy Reviews (2020) **3** (2), 286
- 145. Hao, Z., et al., Nano Energy (2017) 40, 360
- 146. Wang, H.-C., et al., Chemistry A European Journal (2017) 23 (40), 9666
- 147. Tian, Y., et al., ACS Appl. Mater. Interfaces (2019) 11 (26), 23271
- 148. Wu, J., et al., Chem. Eng. J. (2019) **370**, 556
- 149. Cheng, S., et al., Chem. Eng. J. (2021) **417**, 128172
- 150. Zhang, H., et al., Adv. Mater. (2021) 33 (21), 2008447
- 151. Xu, L., et al., Angew. Chem. Int. Ed. (2019) **58** (33), 11491
- 152. Lin, H., et al., ACS Nano (2019) 13 (6), 7073
- 153. Wang, H.-E., et al., J. Mater. Chem. A (2019) 7 (19), 12068
- 154. Zhang, Q., et al., Appl. Surf. Sci. (2019) 487, 452
- 155. Lin, H., et al., Energy Environ. Sci. (2017) 10 (6), 1476
- 156. Yi, Y., et al., Chemistry A European Journal (2019) **25** (34), 8112
- 157. Shen, Z., et al., ACS Nano (2020) 14 (6), 6673
- 158. Tian, Y., et al., Adv. Mater. (2020) **32** (4), 1904876
- 159. Yang, J., et al., Nanoscale (2020) 12 (7), 4645
- 160. Zhang, Y., et al., Adv. Funct. Mater. (2020) 30 (22), 2001165
- 161. Li, Z., et al., Nano Energy (2021) 89, 106331
- 162. Zhang, Y., et al., Adv. Mater. (2020) 32 (7), 1905923
- 163. Yan, D., et al., Adv. Mater. (2017) **29** (48), 1606459
- 164. Jin, J., et al., J. Mater. Chem. A (2020) 8 (6), 3027
- 165. Zhou, T., et al., Nano Energy (2017) 39, 291
- 166. Ye, Z., et al., Adv. Mater. (2020) 32 (32), 2002168
- 167. Zhang, Y., et al., Angew. Chem. Int. Ed. (2021) n/a (n/a)

https://doi.org/10.1002/anie.202108882

- 168. Zeng, S., et al., Small (2020) 16 (39), 2001027
- 169. Gao, X., et al., Adv. Funct. Mater. (2019) 29 (8), 1806724
- 170. He, J., et al., Energy Environ. Sci. (2019) 12 (1), 344
- 171. Zhang, Z., et al., Matter (2020) 3 (3), 920
- 172. Liu, S., et al., ACS Nano (2020) **14** (7), 8220
- 173. Wang, S., et al., Adv. Energy Mater. (2021) 11 (11), 2003314
- 174. Zhou, T., et al., Energy Environ. Sci. (2017) 10 (7), 1694
- 175. Ji, L., et al., Adv. Funct. Mater. (2020) **30** (28), 1910533
- 176. Song, Y., et al., Energy Environ. Sci. (2018) **11** (9), 2620
- 177. Zhang, L., et al., ACS Nano (2020) 14 (7), 8495
- 178. Ye, C., et al., Angew. Chem. Int. Ed. (2018) **57** (51), 16703
- 179. Zhang, B., et al., Adv. Energy Mater. (2020) 10 (15), 2000091
- 180. Wang, M., et al., ACS Nano (2019) 13 (11), 13235
- 181. Hu, L., et al., Adv. Energy Mater. (2018) 8 (23), 1800709
- 182. Wang, M., et al., Chemistry A European Journal (2019) 25 (21), 5416
- 183. Li, W., et al., J. Mater. Chem. A (2020) 8 (1), 433
- 184. Yao, W., et al., ACS Nano (2021) 15 (4), 7114
- 185. Fang, R., et al., Energy Storage Mater. (2018) 10, 56
- 186. Zhang, Y., et al., InfoMat (2021) 3 (7), 790
- 187. Wang, Y., et al., Adv. Energy Mater. (2019) 9 (24), 1900953
- 188. Zhao, C., et al., Nat. Nanotechnol. (2021) 16 (2), 166
- 189. Wang, Y., et al., Energy Environ. Sci. (2020) **13** (11), 3848
- 190. Du, W., et al., Nano-Micro Lett. (2021) 13 (1), 50
- 191. Jiang, M., et al., J. Energy Chem. (2021) **58**, 300

192. Eshetu, G. G., et al., J. Am. Chem. Soc. (2018) **140** (31), 9921

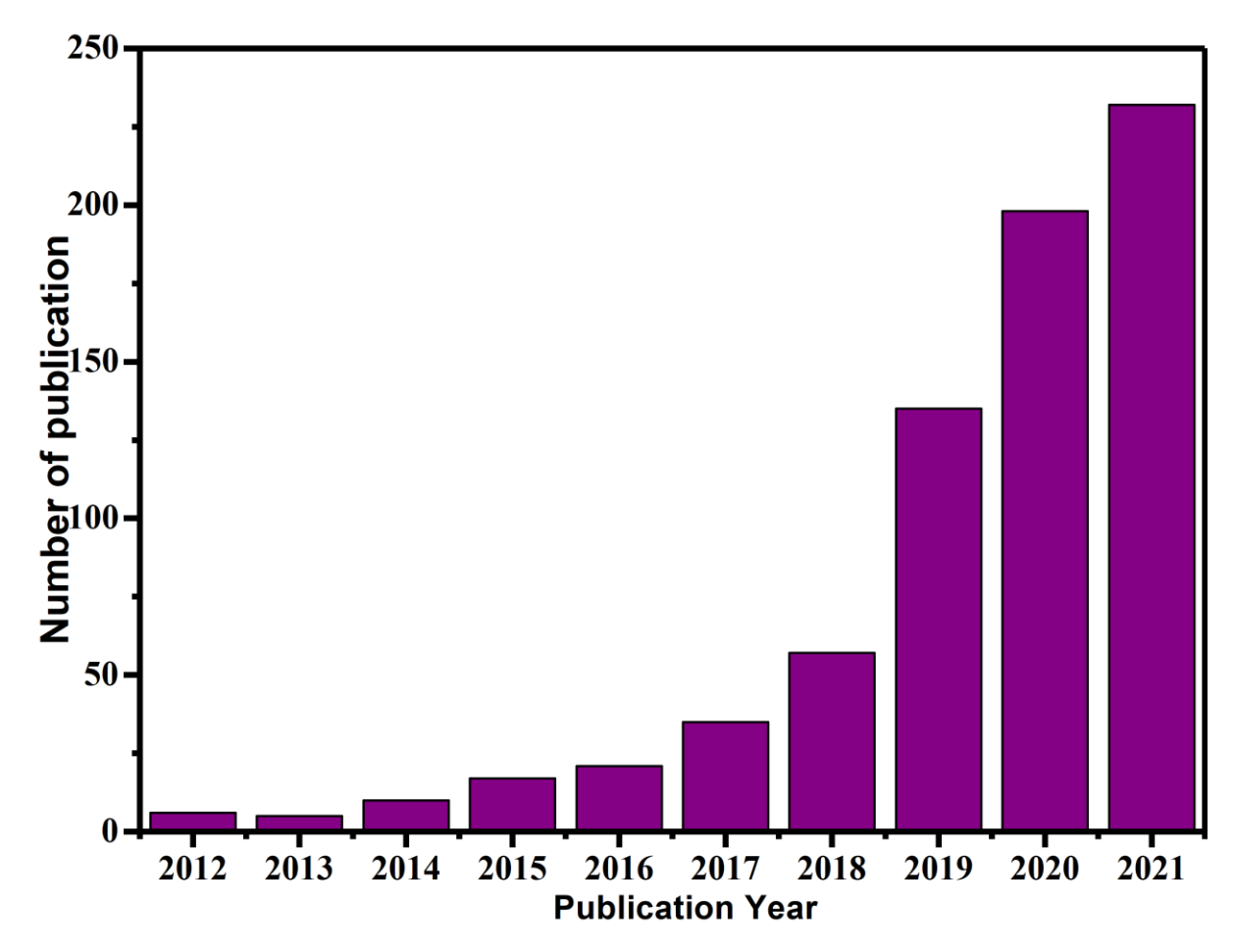


Figure 1. Publication trend related to the catalytic process in LSBs over the last 10 years. (Source: Web of Science, resulting from the search of "lithium sulfur" and "catalytic" as "Topic", retrieved on 25 September 2021)

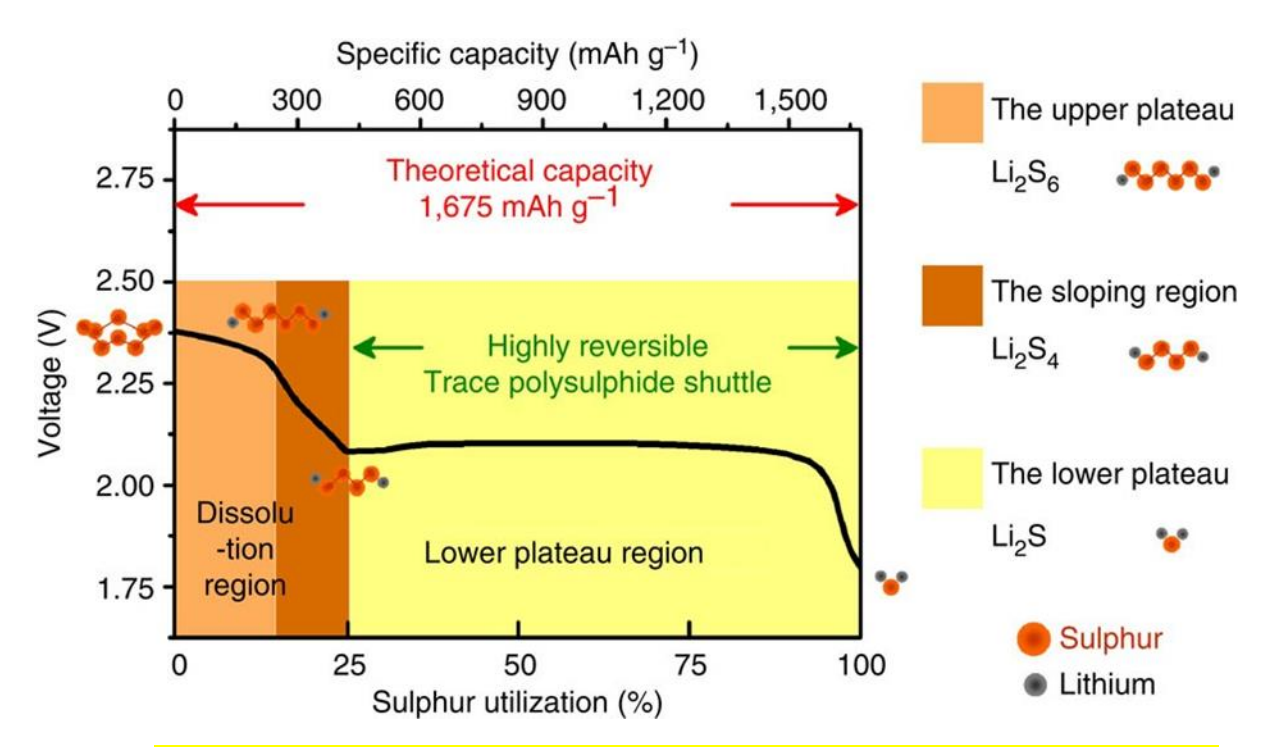


Figure 2. The discharge reaction mechanism of an LSB. During a discharging process, the discharge curve can be divided into two main regions: the upper plateau and the sloping region are located in the dissolution region, and the lower plateau is located in the lower plateau region that provides highly reversible capacity and has only a negligible amount of polysulfide shuttle behaviour. Printed with permission from²². Copyright 2013, Nature Publishing Group.

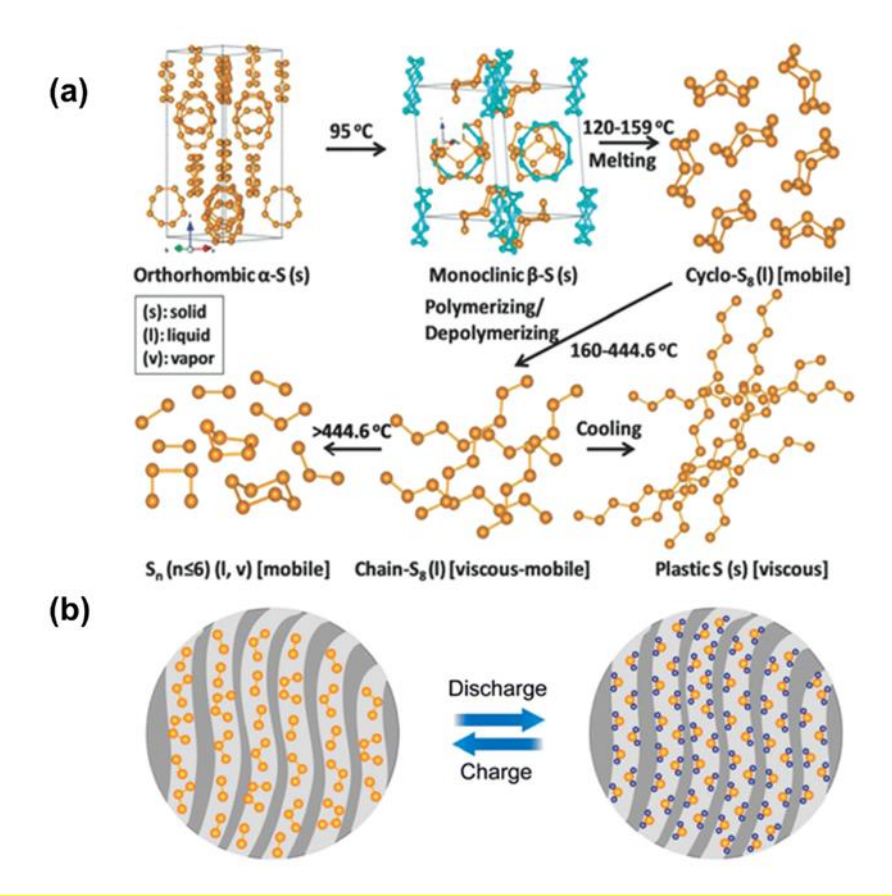


Figure 3. The sulfur allotropes for LSBs. (a) Schematic illustration of structural transformation of various sulfur allotropes. Printed with permission from⁴². Copyright 2013, Royal Society of Chemistry. (b) Schematic illustration of small sulfur molecules of S₂₋₄ and Li₂S confined in a conductive microporous carbon matrix. Printed with permission from²⁸. Copyright 2012, American Chemical Society.

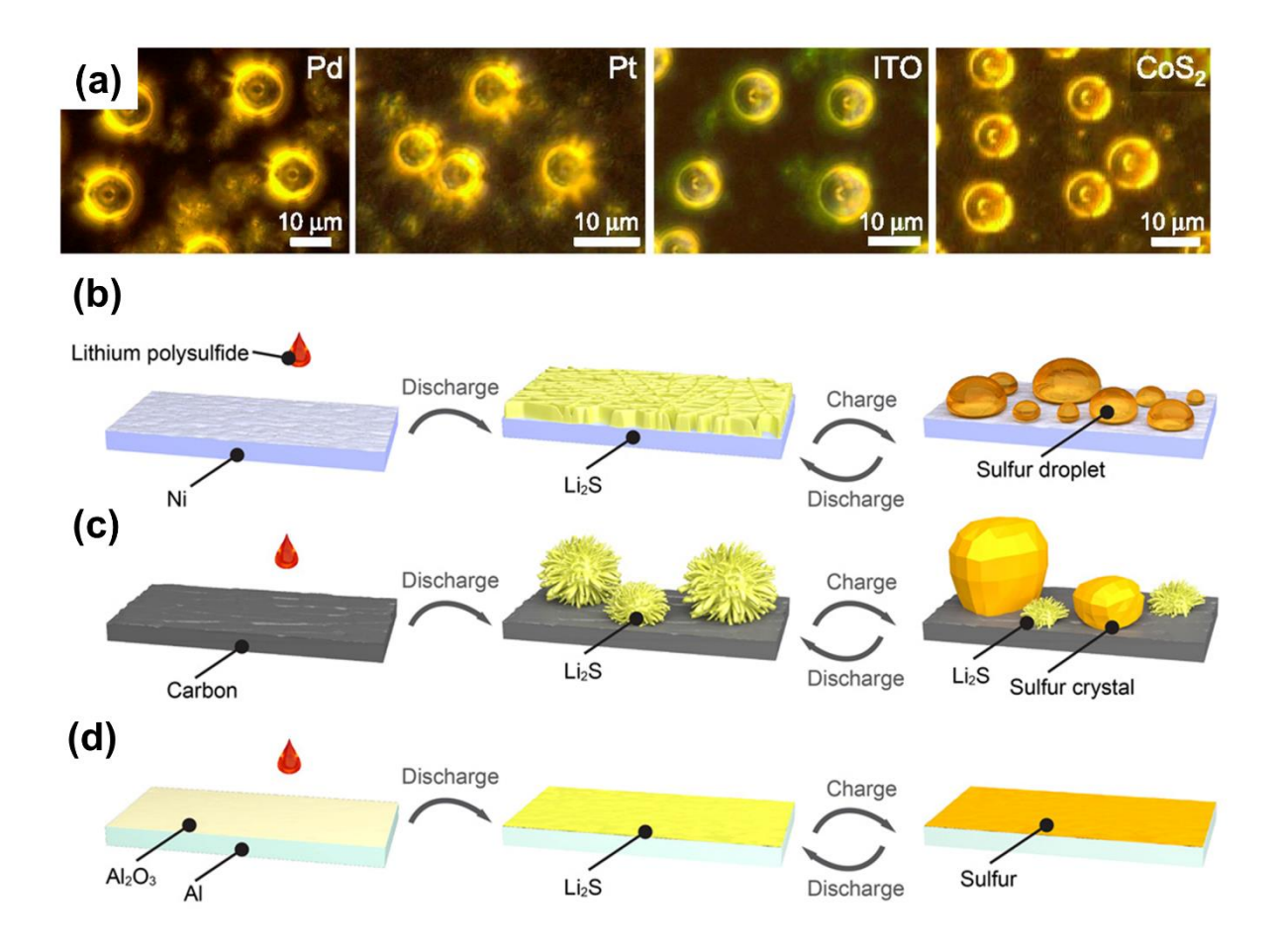


Figure 4. The supercooled sulfur and its application in LSBs. (a) *In operando* dark-field light microscopy (DFLM) images of sulfur droplets electrochemically formed on Pd, Pt, ITO, and CoS₂ substrates. Printed with permission from⁴⁴. Copyright 2019, National Academy of Sciences. (b-d) Schematic illustration of the sulfur species evolution on different substrates during charging and discharging processes. Printed with permission from²⁵. Copyright 2020, American Association for the Advancement of Science.

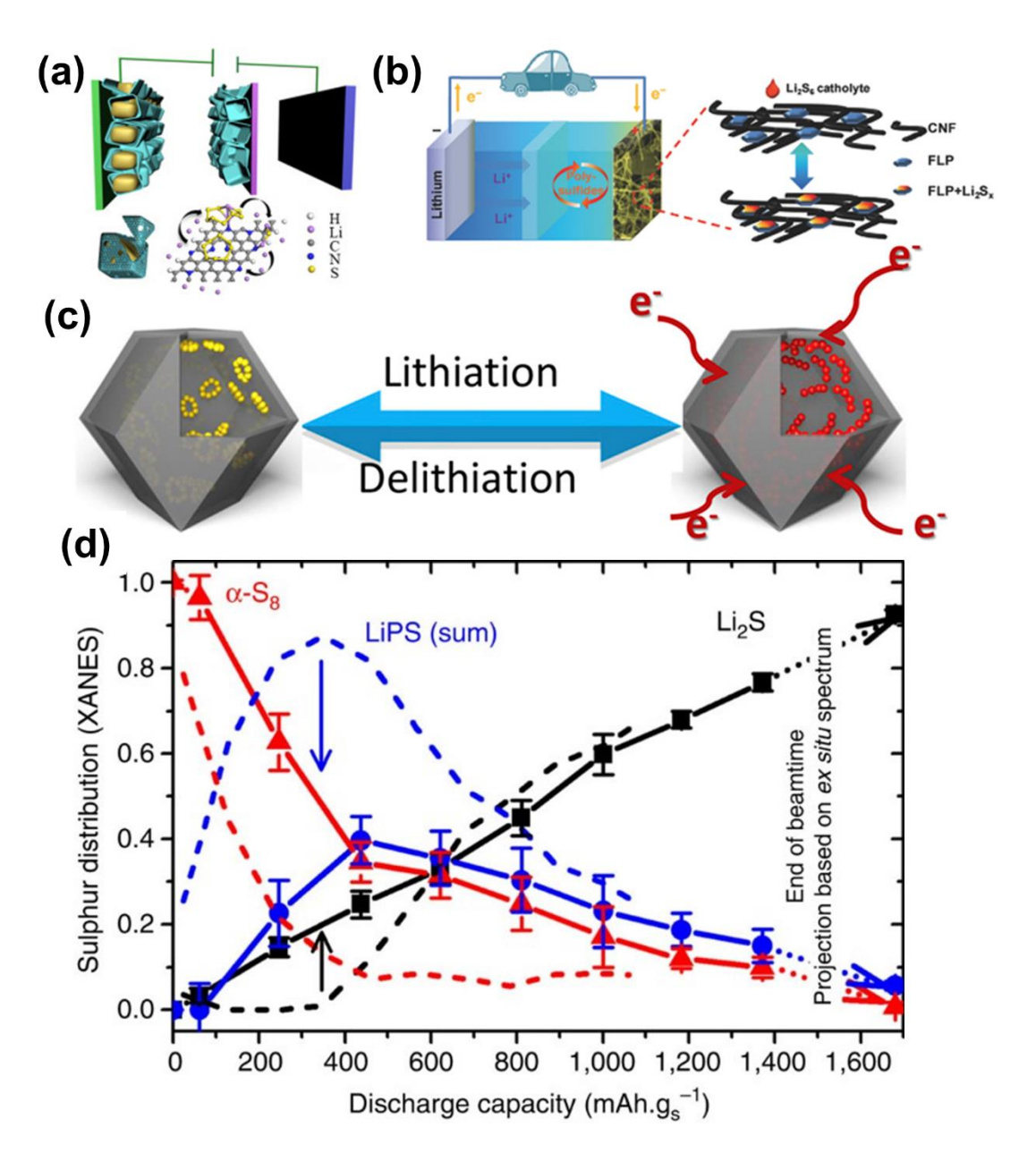


Figure 5. The conductive catalytic materials in LSBs. (a) Schematic illustration of the hierarchical nitrogen-doped carbon nanocages (hNCNC) as host and interlayer in LSBs. Printed with permission from⁵⁵. Copyright 2019, Elsevier. (b) Schematic illustration of the few-layer phosphorene nanosheets-carbon nanofibre (FLP-CNF) as the host in LSBs. Printed with permission from⁵⁷. Copyright 2016, John Wiley and Sons. (c) Schematic illustration of the trapping mechanism of S and Li₂S_x in hollow porous B, N-co-doped graphitic carbon-Co composite (h-Co-BN-GC). Printed with permission from⁵⁸. Copyright 2019, Elsevier. (d) Distribution of sulfur species upon discharge determined by *operando* X-ray absorption near-edge spectroscopy (XANES). Printed with permission from⁶³. Copyright 2014, Nature Publishing Group.

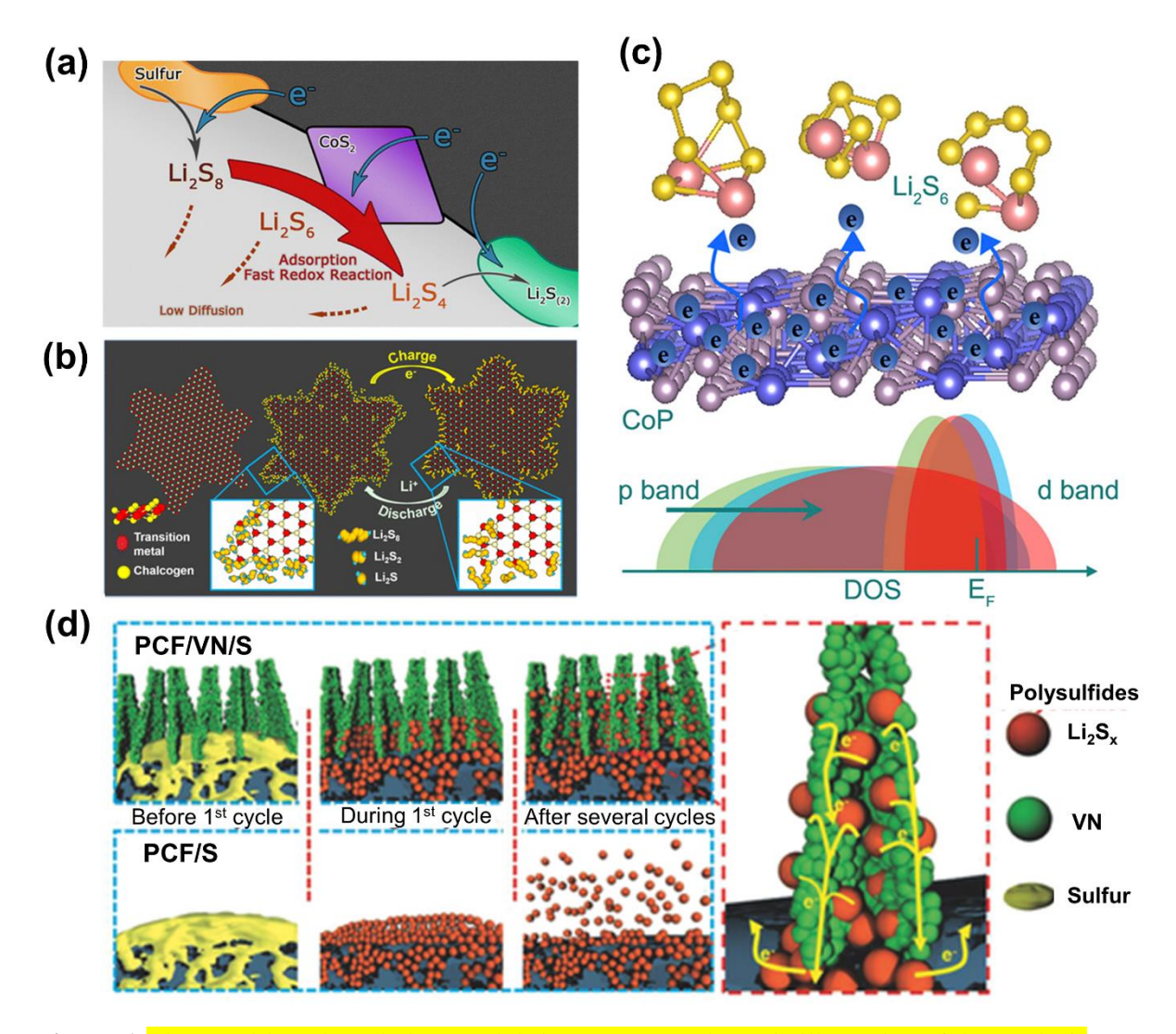


Figure 6. The metal-based catalytic materials in LSBs. (a) Schematic illustration of the catalysis mechanisms of CoS₂ in LSBs. Printed with permission from²⁰. Copyright 2016, American Chemical Society. (b) Schematic illustration of chemical vapor deposition-grown transition metal dichalcogenide nanosheets for LSBs. Printed with permission from⁸³. Copyright 2017, American Chemical Society. (c) Schematic illustration of p bands originating from the non-metal anions in CoP modulating the interfacial redox reaction dynamics by tuning the electron energy of the valence band. Printed with permission from¹⁰⁰. Copyright 2018, Elsevier. (d) Schematic illustration of dual blocking effects associated with "physical block and chemical absorption" for polysulfides in the porous carbon fibers/vanadium nitride array (PCF/VN)/S electrode. Printed with permission from¹⁰³. Copyright 2018, John Wiley and Sons.

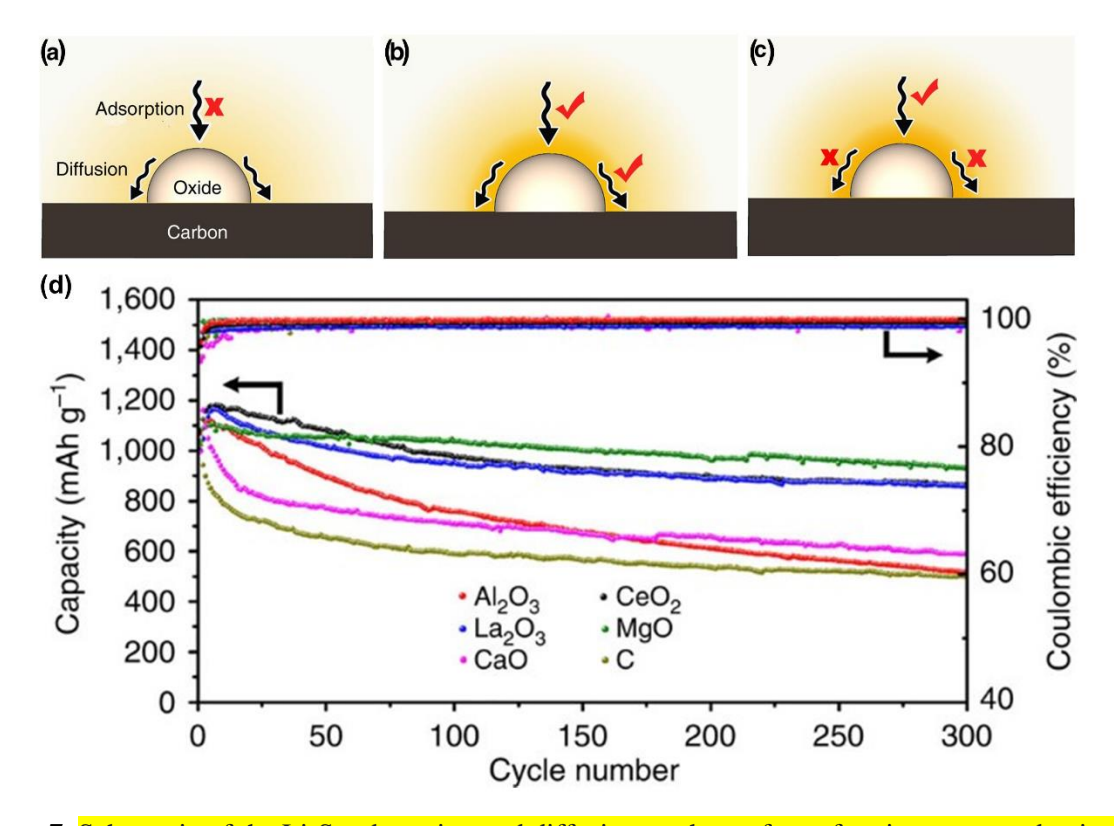


Figure 7. Schematic of the Li₂S_x adsorption and diffusion on the surface of various nonconductive metal oxides. (a) The metal oxide with weak Li₂S_x adsorption capability; only few Li₂S_x can be captured by the oxide; (b) The metal oxide with both strong adsorption and good diffusion, which is favourable for the electrochemical reaction and the controllable deposition of sulfur species; (c) The metal oxide with strong bonding but without good diffusion; the growth of Li₂S and the electrochemical reaction on the oxide/C surface is impeded. (d) Specific capacity and the corresponding Coulombic efficiency of the composite electrodes upon prolonged 300 chargedischarge cycles at 0.5 C. Printed with permission from 104. Copyright 2016, Nature Publishing Group.

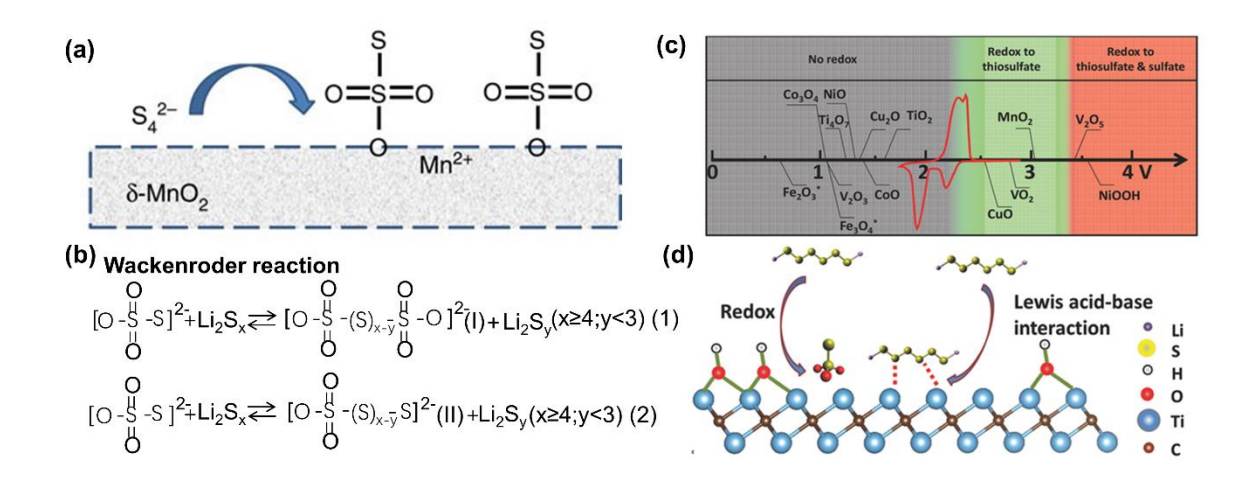


Figure 8. The catalysis mechanisms are relying on mediating polysulfide redox through insoluble thiosulfate species. (a) Schematic illustration of the oxidation of initially formed polysulphide by δ-MnO₂ to form thiosulfate on the surface, concomitant with the reduction of Mn⁴⁺ to Mn²⁺. (b) Proposed reaction mechanisms of polysulfide reduction to form an intermediate polythionate complex and shorter-chain polysulfides. Printed with permission from¹⁰⁵. Copyright 2015, Nature Publishing Group. (c) The chemical reactivity of different metal oxides with LiPSs as a function of redox potential versus Li/Li⁺, superimposed with a typical Li-S cyclic voltammetry curve (shown in red). Printed with permission from¹⁰⁶. Copyright 2015, John Wiley and Sons. (d) Schematic demonstrating the two-step interaction between a representative hydroxyl-decorated MXene phase and polysulfides. Printed with permission from¹⁰⁷. Copyright 2016, John Wiley and Sons.

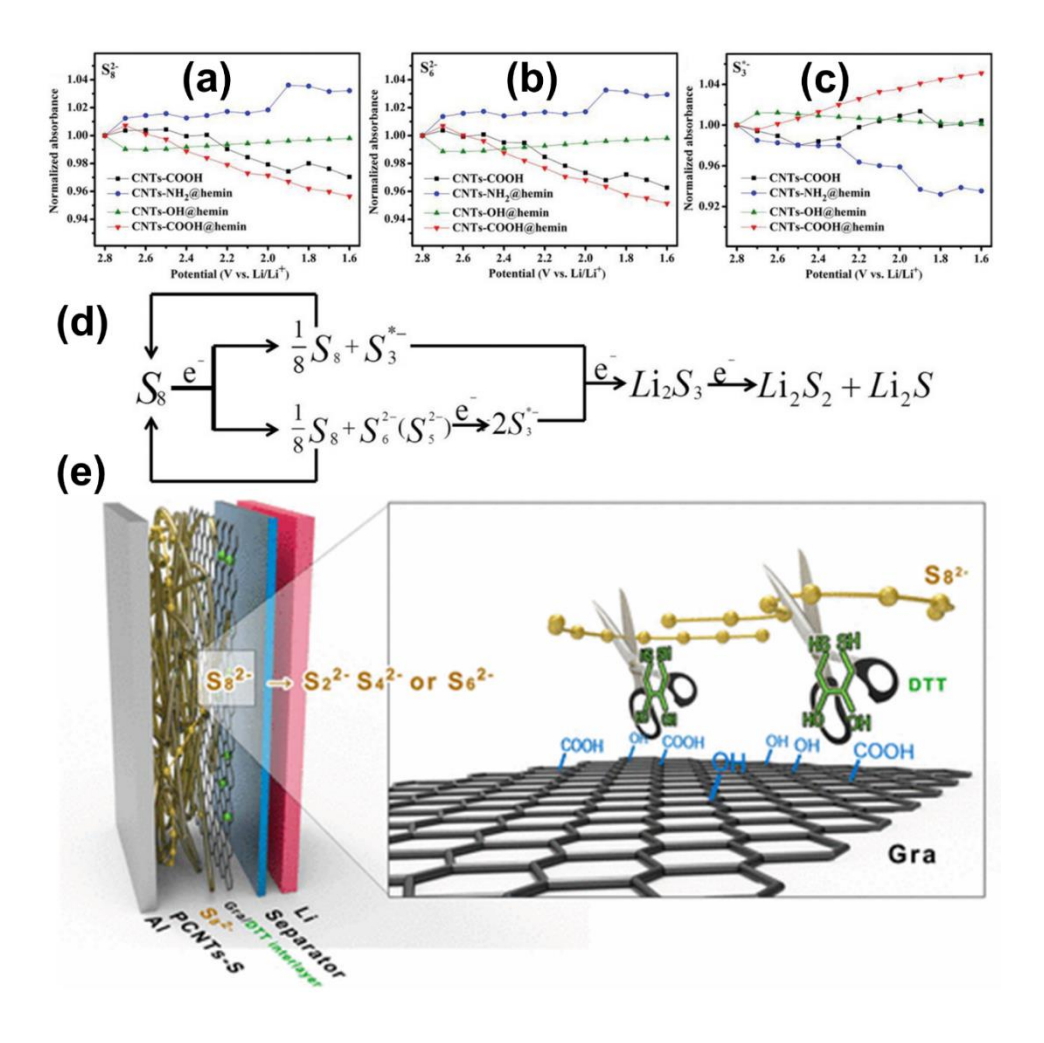


Figure 9. Disulfide bond cleavage to design the LiPSs molecular structure. (a-d) *In-situ* UV-vis spectroscopic study showing the normalized absorbance of S₈²⁻(a), S₆²⁻(b), and S₃*- (c) as a function of potential at different electrode surfaces during discharge and the proposed sulfur reduction reaction pathways in our Li-S battery (d). Printed with permission from 112. Copyright 2020, John Wiley and Sons. (e) Schematic illustration of graphene/dithiothreitol (Gra/DTT) interlayer in LSBs. Printed with permission from 114. Copyright 2017, American Chemical Society.

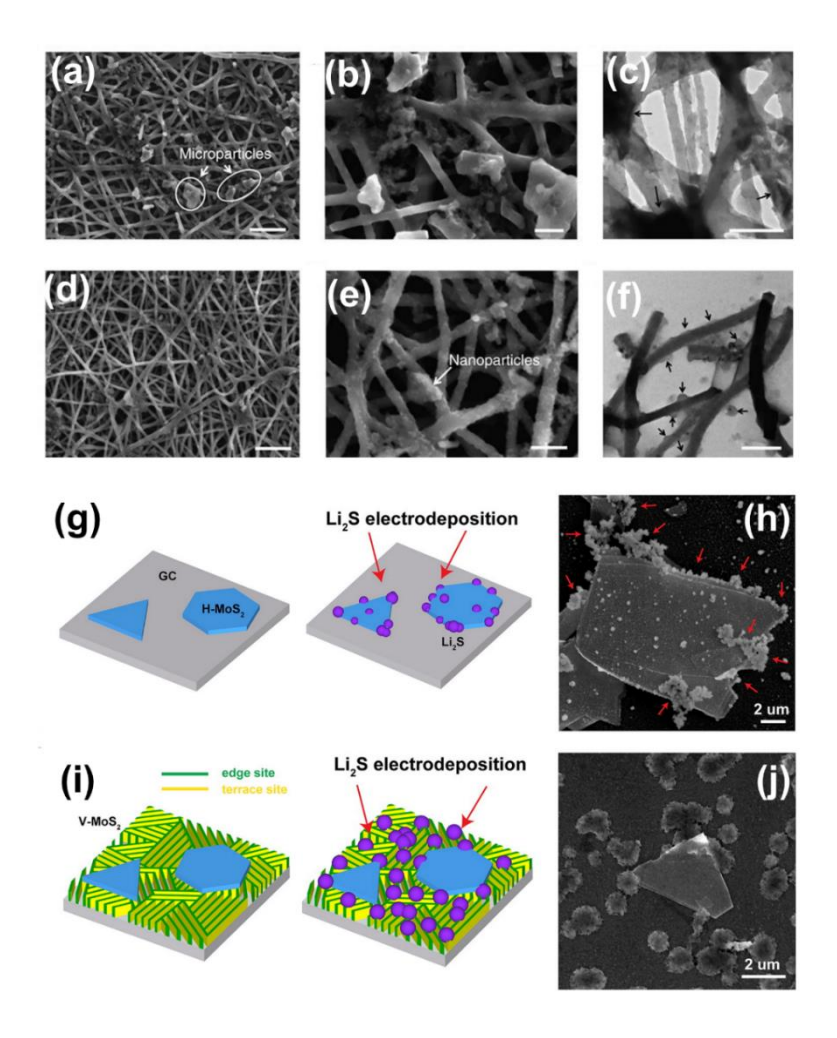


Figure 10. The regulation of Li₂S growth via deposition sites on catalytic materials. (a-f) The morphology of a carbon nanofiber electrode (a-c) and tin-doped indium oxide coated carbon nanofibers (ITO-C) nanofiber electrode (d-f) after discharge showing the microparticles formed on the nanofiber electrode. (a, d) Scale bar, 2 μm. (b, c, e, f) Scale bar, 500 nm. Printed with permission from 117. Copyright 2014, Nature Publishing Group. (g, h) Schematic illustration (g) and SEM image (h) of H-MoS₂ nanosheets on glassy carbon (GC) substrate with Li₂S electrodeposition. Li₂S nanoparticles tend to be deposited onto the MoS₂ edge sites. (i, j) Schematic illustration (i) and SEM image (j) of H-MoS₂ nanosheet on edge-terminated V-MoS₂ nanofilm. Li₂S nanoparticles are attracted by the MoS₂ edges on the substrate. Printed with permission from 118. Copyright 2014, American Chemical Society.

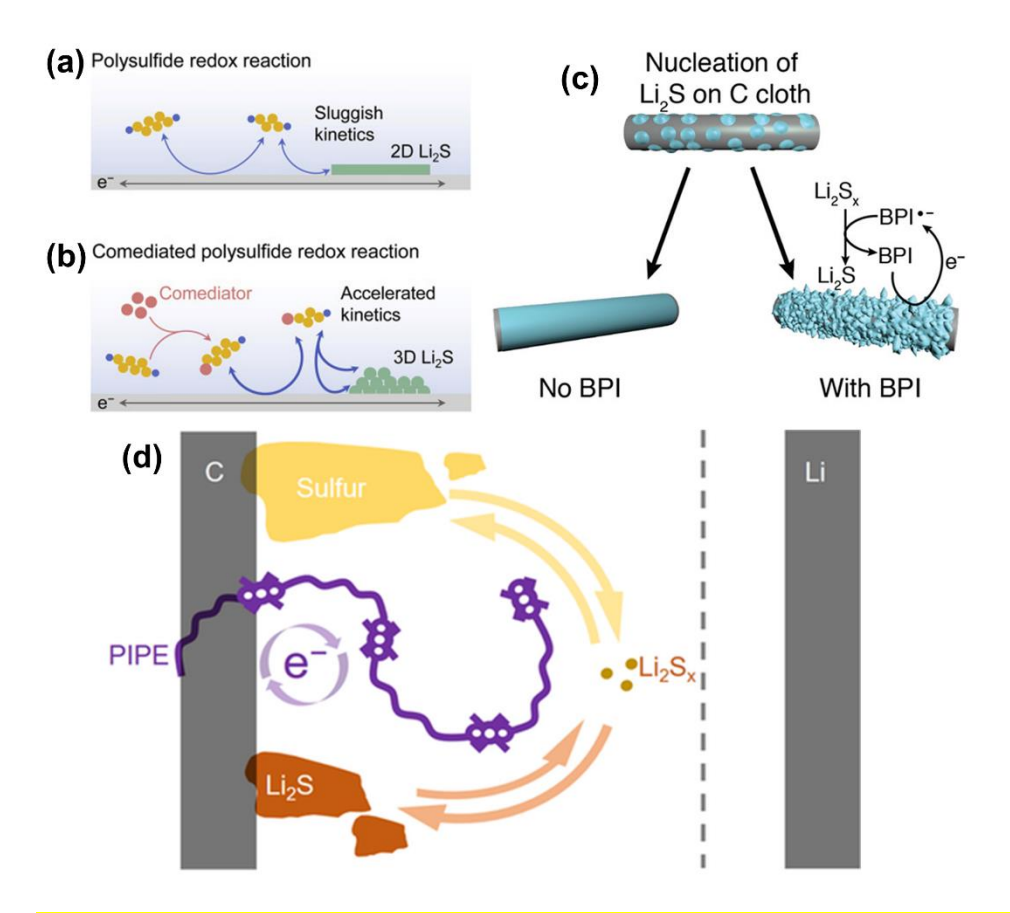


Figure 11. The regulation of Li₂S growth via LiPSs mediators. (a, b) Schematic illustration of the polysulfide-mediated reaction pathway for routine Li-S batteries (a) and the redox-mediated reaction pathway (b). Printed with permission from¹²⁰. Copyright 2020, Elsevier. (c) Schematic representation of the electrodeposition of Li₂S onto carbon cloth in the absence (left) and presence (right) of benzo[ghi]peryleneimide (BPI). Printed with permission from¹²¹. Copyright 2016, American Chemical Society. (d) Schematic illustration of polyimide-polyether (PIPE) to regulate the electron transfer reaction between sulfur, polysulfides, and sulfides on conductive surfaces. Printed with permission from¹²². Copyright 2020, John Wiley and Sons.

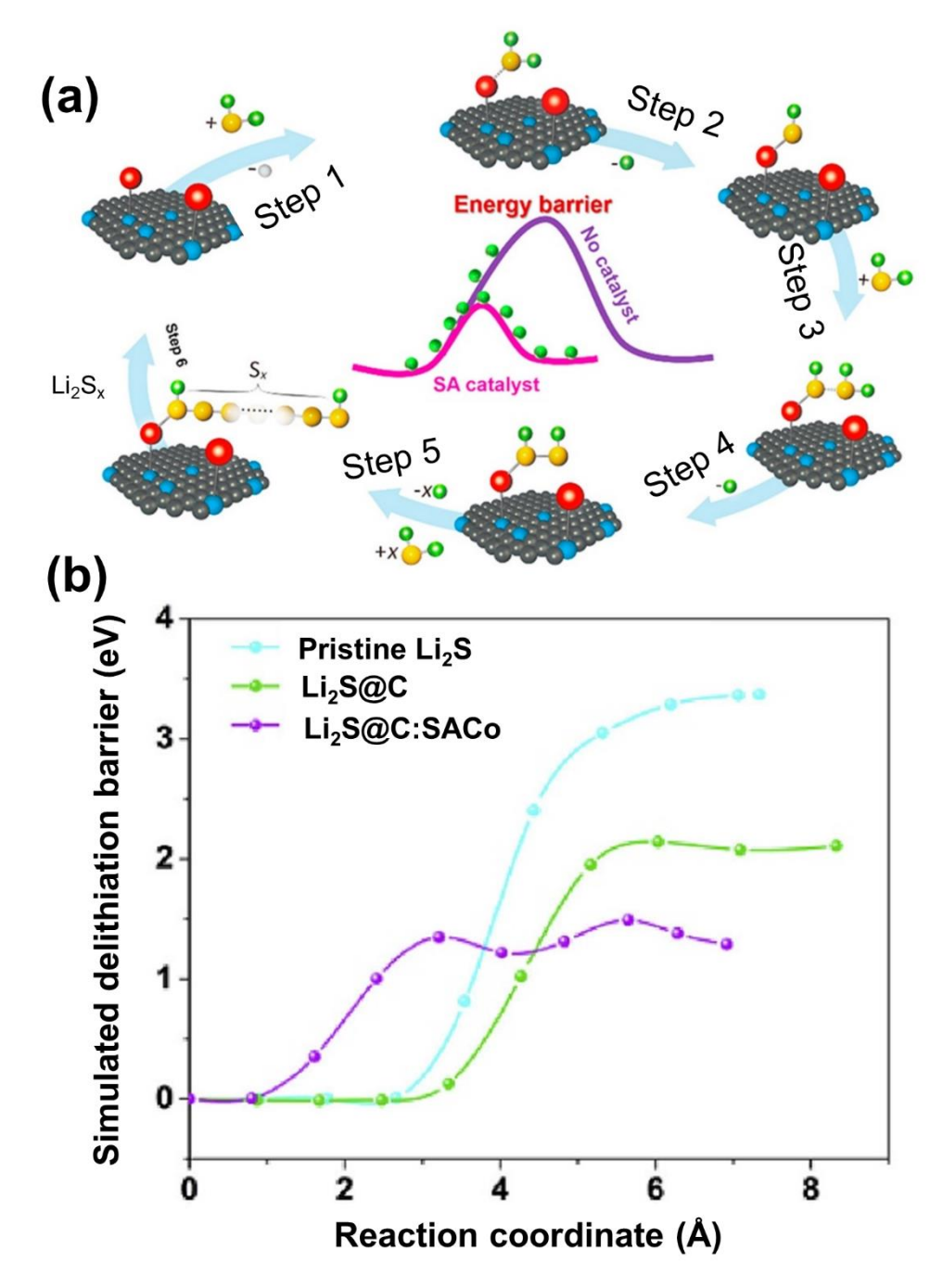


Figure 12. The working mechanisms of single atomic catalysts (SACs) in LSBs. (a) Schematic illustration of single iron atoms (SAFe) to catalyse Li₂S delithiation. Printed with permission from ¹³². Copyright 2019, Elsevier. (b) Comparison of simulated delithiation energy barrier of Li₂S on pristine Li₂S, Li₂S@C and L₂S@C:SACo matrices. Printed with permission from ¹³³. Copyright 2020, Elsevier.

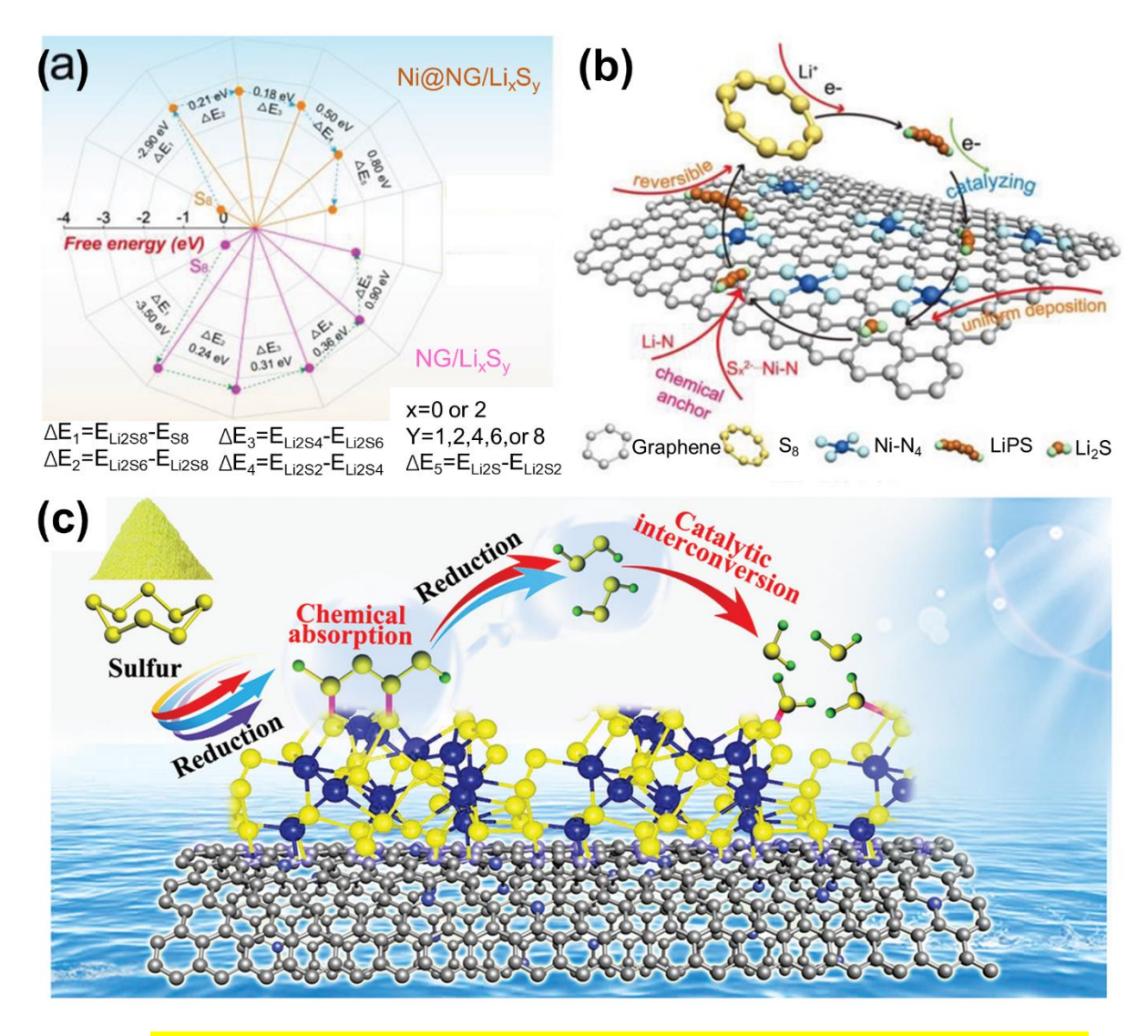


Figure 13. The representative catalytic materials to catalyse Li₂S₂-Li₂S conversion. (a, b) The free-energy diagrams of LiPS on the surface of single nickel (Ni) atoms on nitrogen-doped graphene (Ni@NG) or nitrogen-doped graphene (NG) (a) and the catalytic mechanism of the LiPS on the surface of Ni@NG in the electrochemical process (b). Printed with permission from 135. Copyright 2019, John Wiley and Sons. (c) Schematic illustration of the reaction process of sulfur on the CoS₃ catalyst. Printed with permission from 143. Copyright 2019, John Wiley and Sons.

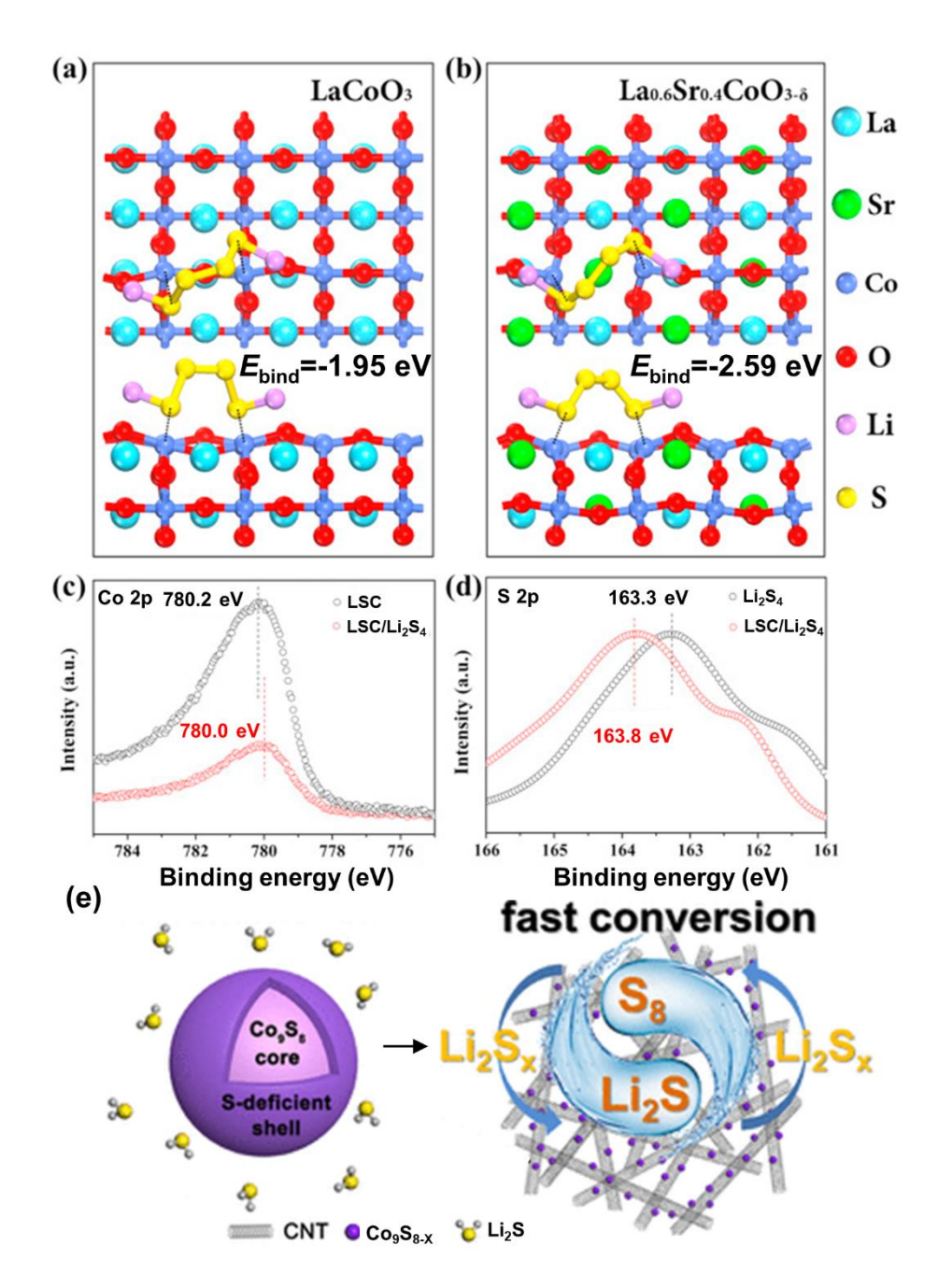


Figure 14. The application of defect engineering in LSBs. (a-d) The most stable adsorption structures, after full relaxation, of Li₂S₄ on LaCoO₃ (110) (a) and La_{0.6}Sr_{0.4}CoO_{3-δ} (110) (b) surfaces, and the XPS spectra of Co 2p (c) and S 2p (d) in LSC, Li₂S₄, and LSC/Li₂S₄ samples. Printed with permission from ¹⁴⁵. Copyright 2017, Elsevier. (e) Schematic illustration of the synthesis of Co₉S_{8-x}/CNT and the conversion of Li₂S_x on the Co₉S_{8-x}/CNT surface. Printed with permission from ¹⁵². Copyright 2019, American Chemical Society.

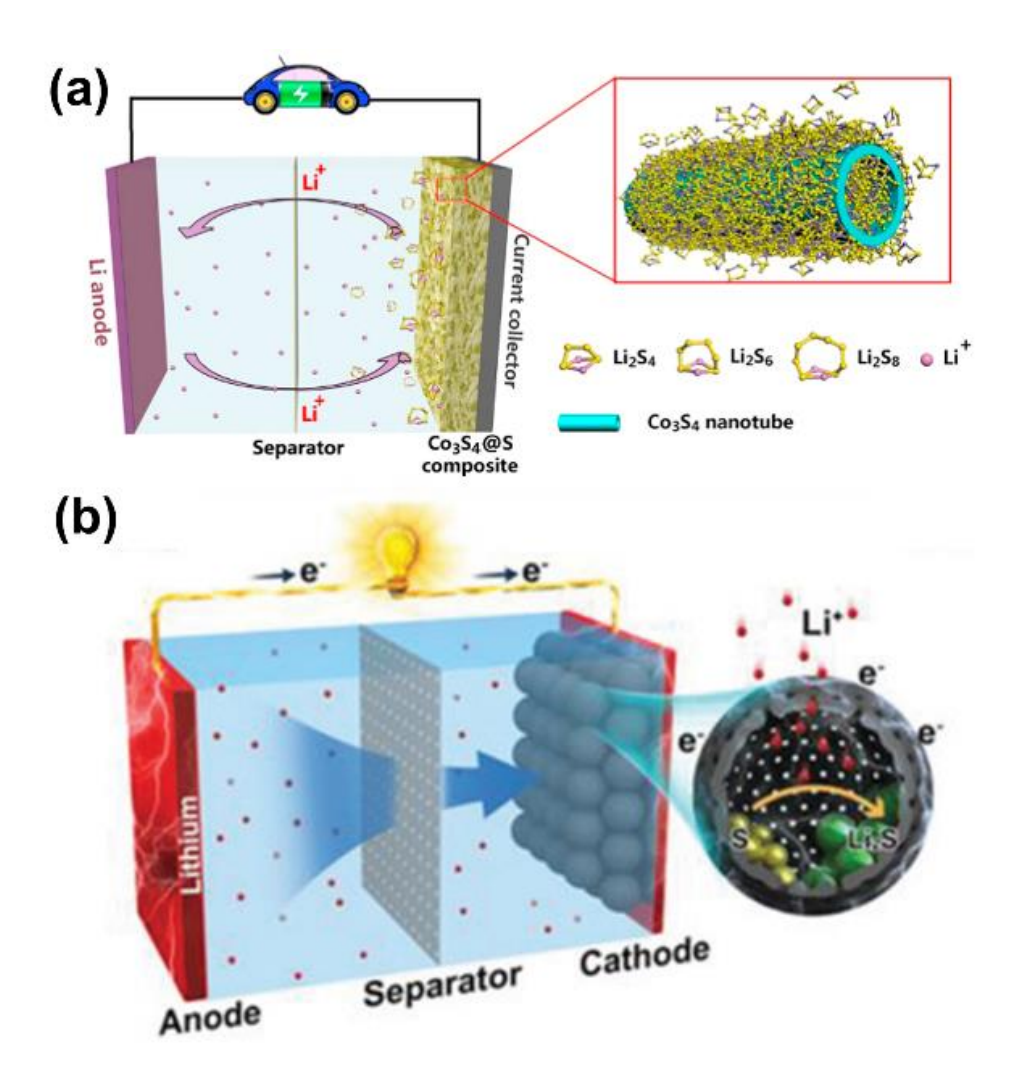


Figure 15. The nano-structure design of catalytic materials for LSBs. (a) Schematic illustration of Co₃S₄@S nanotube composite to minimize the shuttle effect of polysulfides in LSBs. Printed with permission from⁷⁸. Copyright 2017, Elsevier. (b) Schematic diagram of sulfur@N-doped porous carbon cages (S@NHSC) cathode for LSBs. Printed with permission from¹⁶⁸. Copyright 2020, John Wiley and Sons.

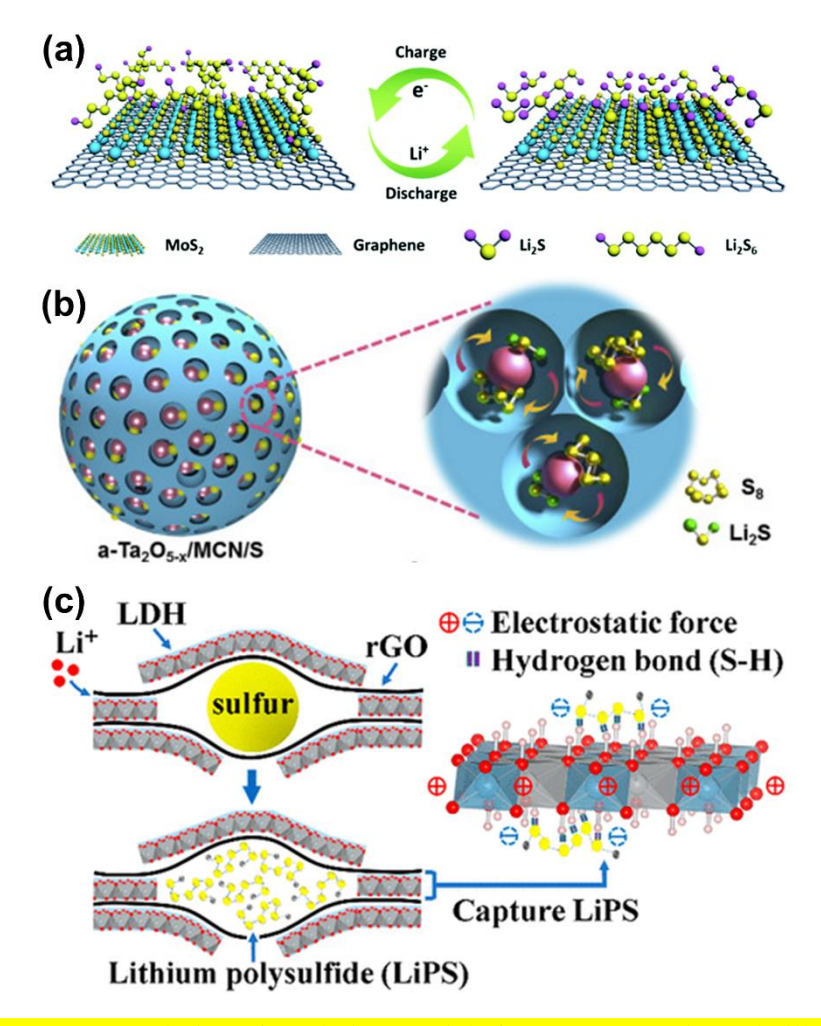


Figure 16. The 3D structure design of catalytic materials for LSBs. (a) Schematic illustration of the conversion process of LiPSs on 3D graphene/1T MoS₂ (3DG/TM) heterostructure as a highly efficient electrocatalyst. Printed with permission from¹⁷⁰. Copyright 2018, Royal Society of Chemistry. (b) Scheme illustration of LiPS catalytic conversion in an ultrafine Ta₂O_{5-x} nanoclusters implanted in micropores of carbon nanospheres (a-Ta₂O_{5-x}/MCN) nanoreactor. Printed with permission from¹⁷¹. Copyright 2020, Elsevier. (c) Schematic illustration of a sulfur nanocrystal and LiPSs embedded in the layered double hydroxide (LDH) layers. Printed with permission from¹⁷². Copyright 2020, American Chemical Society.

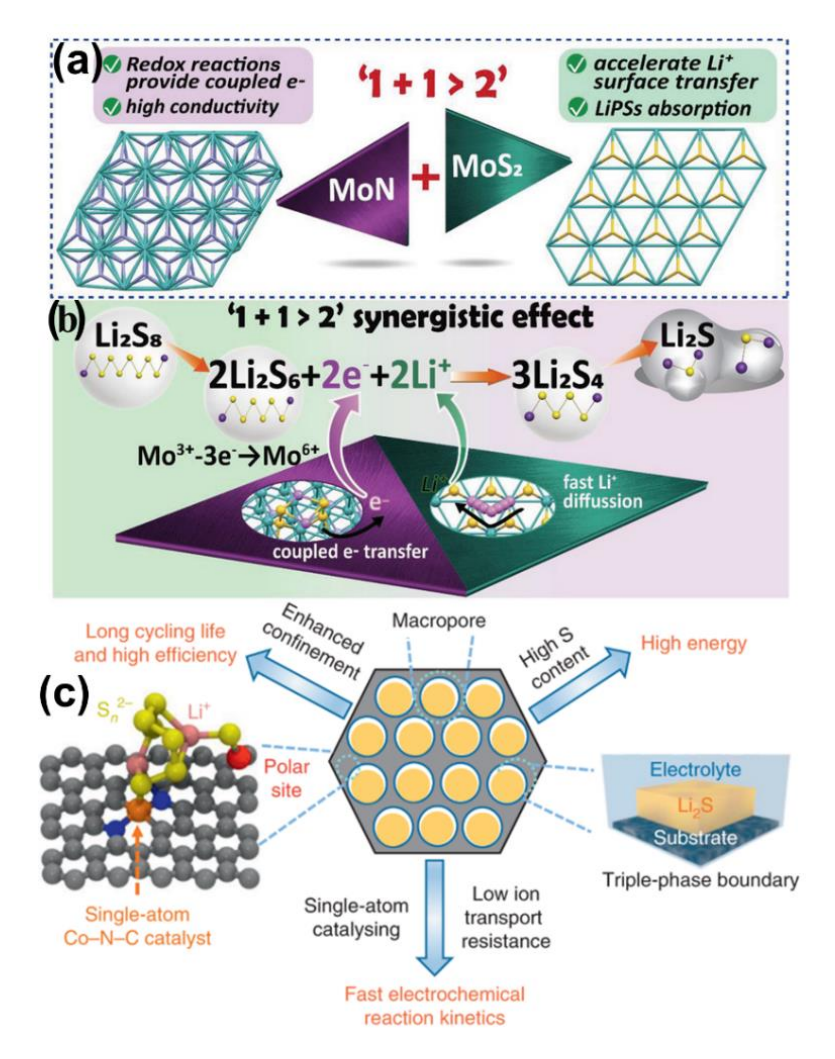
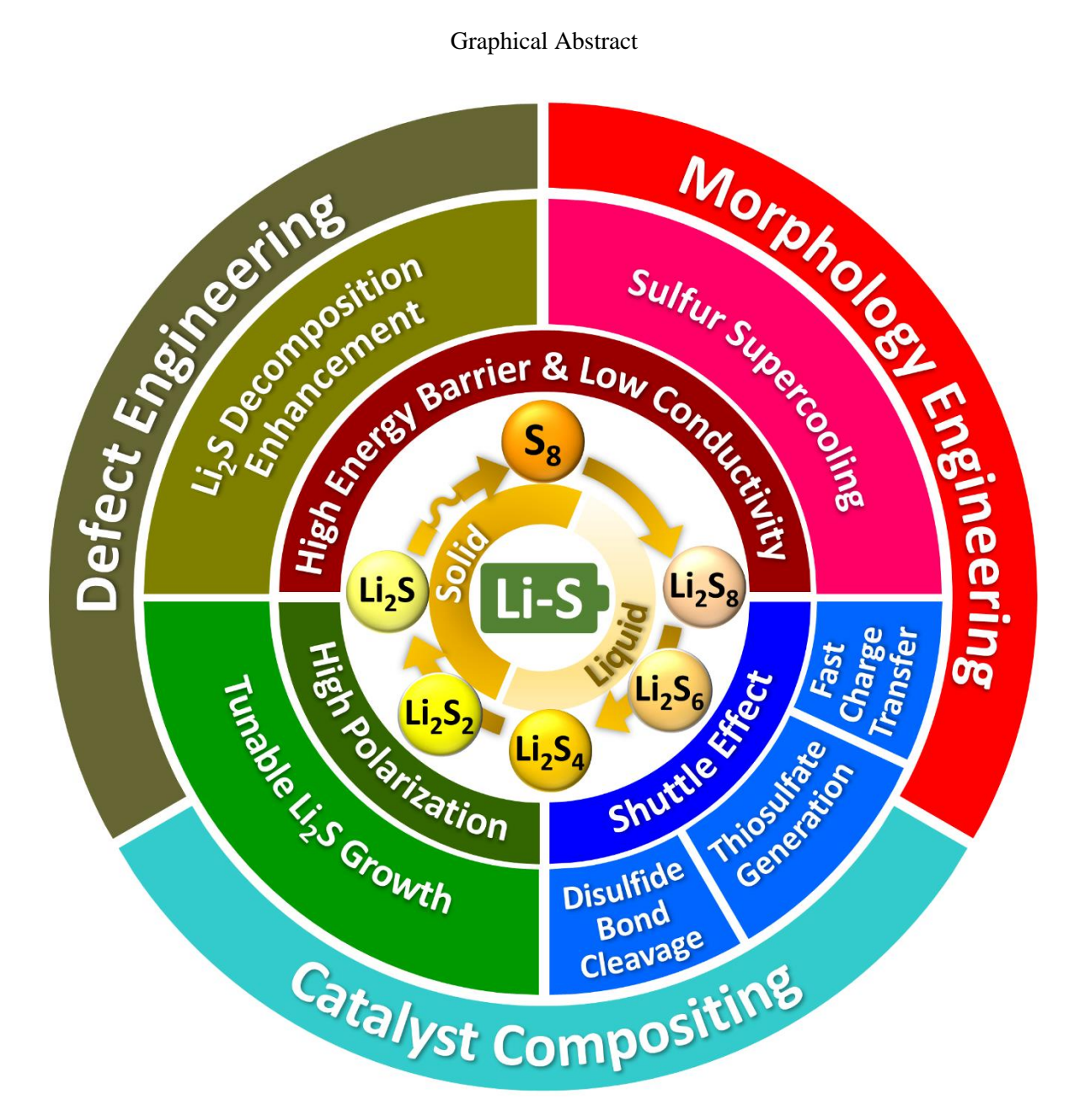


Figure 17. The design strategy of composite catalysts for LSBs. (a, b) Schematic illustration of heterostructure MoS₂-MoN host (a) and synergistic catalytic conversion of LiPSs by the MoS₂-MoN host during the charge/discharge processes (b). Printed with permission from ¹⁷³. Copyright 2021, John Wiley and Sons. (c) Schematic illustration of the cobalt in nitrogen-doped graphene (Co-N-C) as single-atom catalyst (SAC) sites and the ZnS polar site to suppress shuttle effect and lithium anode corrosion. Printed with permission from ¹⁸⁸. Copyright 2021, Nature Publishing Group.

Table 1. Comparison of the electrochemical performance of LSBs using different catalytic materials

Catalytic materials	Sulfur loading	Rate capability	Cycling performance	Ref.
Catalytic materials	(mg/cm ²)	(mAh/g)	(mAh/g)	Kei.
3D Ni foam	<mark>4.8</mark>	450/2C	$\sim 652/200^{\text{th}} (0.5\text{C})$	25
hNCNC	<mark>0.8</mark>	539/20A/g	$438/1000^{\text{th}} (10A/g)$	<mark>55</mark>
BP	2 3.3	784/4C	589/1000 th (2C)	<mark>56</mark>
<mark>FLP</mark>	<mark>3.3</mark>	<mark>785/3C</mark>	660/500 th (1C)	<mark>57</mark>
<mark>h-Co-BN-GC</mark>	1.3-1.4	<mark>705/2C</mark>	877/ 500 th (0.5C)	<mark>58</mark>
$\overline{ ext{Ti}_4 ext{O}_7}$	1.5-1.8	850/2C	~940/100 th (0.5C)	<mark>63</mark>
MXene-CNT	NA	<mark>686/8C</mark>	610/500 th (1C)	<mark>71</mark>
${\color{red}{ m CoS_2}}$	<mark>0.4</mark>	1003/2C	320.96/2000 th (2C)	<mark>20</mark>
${ m WS}_2$	<mark>NA</mark>	380/1C	652/100 th (0.2C)	<mark>83</mark>
Ni ₂ P	<mark>2</mark>	812/2C	1176/300 th (0.2C)	<mark>86</mark>
${ m W_2C}$	1.77	646/2C	1128/200 th (0.2C)	<mark>87</mark>
<mark>Fe₃C</mark>	<mark>0.7-1</mark>	580.5/4C	721.8/100 th (0.5C)	<mark>89</mark>
<mark>TiN</mark>	1.5-2	701/3C	745.68/450 th (0.5C)	<mark>90</mark>
Co ₄ N	1.5-2	882/2C	$805/300^{th}$ (2C)	<mark>93</mark>
${ m Co_2B}$	<mark>3.6</mark>	1172.8/5C	919/3000 th (5C)	<mark>98</mark>
MnO ₂	0.7-1.0	950/1C	1030/200 th (0.2C)	105
CNTs-COOH@hemin	<mark>NA</mark>	873.4/3C	205/1800 th (1C)	112
<mark>DTT</mark>	<mark>0.49</mark>	712/5C	$301/1100^{th}$ (5C)	<mark>114</mark>
<mark>ITO</mark>	<mark>2</mark>	1050/1C	710/500 th (0.2C)	117
V-MoS ₂ -CN	2 2 1.2	1066/1C	~1000/200 th (1C)	118
<mark>DtbDS</mark>	1.2	<mark>566/4C</mark>	600/300 th (0.5C)	120
<mark>PIPE</mark>	1.3	416/3C	915/300 th (0.5C)	<mark>122</mark>
InI ₃	<mark>2.4</mark>	<mark>736/1.5C</mark>	NA	<mark>130</mark>
<mark>SAFe</mark>	2.0-2.3	588/12C	315/1000 th (5C)	<mark>132</mark>
<mark>SACo</mark>	1.5-2.0	441/10C	280/1500 th (2C)	<mark>133</mark>
$C_{09}S_{8}$	<mark>2</mark>	604/20A g ⁻¹	$605/1000^{\text{th}} (1\text{A g}^{-1})$	<mark>142</mark>
Ni@NG	<mark>1.5</mark>	612/10C	826.2/500 th (1C)	<mark>135</mark>
CoS₃	<mark>6</mark>	1601/0.13C	61047/70 th (0.13C)	143
${ m Sb_2Se_{3-x}}$	<mark>1.8</mark>	<mark>787/8C</mark>	847/500 th (1C)	<mark>158</mark>
CoP	<mark>2.0</mark>	930.1/3 <mark>C</mark>	888/500 th (2C)	<mark>164</mark>
TiO ₂ -TiN	1.0-1.2	682/2C	927/300 th (0.3C)	<mark>174</mark>
WS_2 - WO_3	1.2	<mark>861/3C</mark>	573.7/500 th (0.5C)	<mark>179</mark>
3d-omsh/ZnS, Co-N-C	<mark>1.2</mark>	~700/5C	700/1000 th (1.6C)	<mark>188</mark>

Graphical Abstract



The design strategies for the catalytic materials, including defect engineering, morphology engineering, and catalyst compositing, facilitate sulfur supercooling, fast charge transfer, thiosulfate generation, disulfide bond cleavage, tuneable Li₂S growth, and Li₂S decomposition enhancement, thereby addressing the challenges of the LSB in terms of high energy barrier and low conductivity of S₈ and Li₂S, severe polysulfide shuttling and high polarization of Li₂S₂/Li₂S deposition.